Article

Not peer-reviewed version

The Dzhanibekov Effect Revisited: Informational Hysteresis, Anisotropic Latency Fields, and Regime Transitions in Torque-Free Rotation

Raoul Bianchetti *

Posted Date: 5 March 2026

doi: 10.20944/preprints202603.0378.v1

Keywords: Dzhanibekov effect; tennis racket theorem; rigid-body dynamics; intermediate-axis instability; Viscous Time Theory (VTT); informational geometry; hysteresis and memory; regime transitions; nonlinear dynamics; numerical validation

 doi:10.20944/preprints202603.0378.v1

Article

The Dzhanibekov Effect Revisited: Informational Hysteresis, Anisotropic Latency Fields, and Regime Transitions in Torque-Free Rotation

Raoul Bianchetti

Information Physics Institute, Genoa, Italy; raoul.bianchetti@informationphysicsinstitute.net

Abstract

The Dzhanibekov effect—also known as the tennis racket theorem in its classical formulation—remains one of the most visually striking and widely circulated demonstrations of rotational instability in torque-free motion. A rigid body spinning about its intermediate principal axis undergoes abrupt, repeated flips that appear paradoxical to non-specialists and counterintuitive even to many trained physicists when encountered as a real-world phenomenon rather than as a textbook theorem. Conventional mechanics accounts for this behavior through the instability of the intermediate axis in Euler's equations; however, this explanation is typically framed as a binary statement ("stable" versus "unstable") and rarely develops a deeper dynamical interpretation of three experimentally salient features: (i) the emergence of highly organized, quasi-periodic flips rather than unstructured chaos; (ii) the strong dependence of the observed flip dynamics on preparation, perturbations, and real-world imperfections; and (iii) the apparent "memory" of the system, which repeatedly returns to similar macroscopic configurations despite inevitable dissipation and microstructural coupling. In this paper, we propose a rigorous reinterpretation of the Dzhanibekov effect within the framework of Viscous Time Theory (VTT), viewing the flip not merely as a consequence of intermediate-axis instability, but as a **coherence-regime transition in an anisotropic informational geometry**. We introduce an informational manifold for rigid-body rotation, in which rotational states evolve along constrained trajectories shaped by anisotropic reconfiguration costs associated with the principal inertia structure and by an effective informational viscosity arising from internal mode coupling and finite-time redistribution. In this picture, the flip is not an instantaneous kinematic accident but a **finite-time transition between metastable corridors of rotational coherence**, with the observed quasi-periodicity emerging as a geometric consequence of navigation along preferred informational pathways. This formulation yields a set of quantitative, testable predictions absent from the standard narrative, including hysteresis under cyclic control of initial conditions, direction-dependent flip thresholds and transition times, metastable latency regimes, and scaling relations linking flip timing to an informational viscosity parameter. To assess these predictions, we perform a comprehensive numerical validation combining high-resolution integration of the Euler equations, ensemble statistics over large sets of perturbations, spectral and structural diagnostics, multi-precision convergence testing, and comparative model analysis. Quantitative analysis demonstrates that informational viscosity produces a **bounded suppression of instability growth (approximately 2–15%)** without altering phase-space topology, integrability, or scaling structure. No chaotic attractors, bifurcation cascades, or nonphysical divergences emerge. The Dzhanibekov instability remains fundamentally geometric, with VTT operating as a **coherent rate-level regulator** rather than a replacement mechanism. This bounded rate modification becomes logarithmically amplified in flip-time statistics, providing a clear and measurable experimental signature. By reframing one of the most iconic "video-paradox" phenomena of classical mechanics as an **informational hysteresis and regime-transition process**, this work provides a mathematically grounded bridge between visible macroscopic dynamics and a general theory of anisotropic, viscous informational evolution. The Dzhanibekov effect thus emerges not only as a pedagogical curiosity,

 doi:10.20944/preprints202603.0378.v1

but as a **quantitative macroscopic laboratory** for probing informational geometry, coherence regimes, and finite-time reconfiguration in real physical systems.

Keywords: Dzhanibekov effect; tennis racket theorem; rigid-body dynamics; intermediate-axis instability; Viscous Time Theory (VTT); informational geometry; hysteresis and memory; regime transitions; nonlinear dynamics; numerical validation

---

1. Introduction

1.1. A Phenomenon that "Looks Impossible"—and Therefore Matters

Few demonstrations in physics have achieved the peculiar status of the Dzhanibekov effect: a short sequence of footage recorded in a weightless environment, showing a seemingly simple object rotating smoothly, then suddenly flipping by approximately 180 degrees, and continuing as if nothing had happened—only to flip again, and again, with striking regularity. For a general audience, the phenomenon appears to violate common sense, as if a hidden torque were acting. And for physicists familiar with the tennis racket theorem, it remains visually striking because it makes a textbook result feel like a physical "glitch" in reality [2,4].

This is precisely why the Dzhanibekov effect matters beyond its role as a pedagogical curiosity. Science is not advanced only by phenomena that are hard to see; it is often advanced by phenomena that are **too easy to see**, yet hard to fully understand [3]. The Dzhanibekov flip has that quality: it is globally recognizable, reproducible, and yet still psychologically—and often conceptually—unsatisfying when reduced to the short statement "instability of the intermediate axis."

The present paper begins from a simple premise: **a correct explanation is not necessarily a complete explanation**. Euler's equations correctly describe torque-free rotation and identify the intermediate axis as unstable [2,3]. But the experience of the Dzhanibekov effect—the organized, repeatable flips, their apparent "timing," and their sensitivity to preparation—suggests that the phenomenon is richer than the usual textbook summary.

1.2. From Poinsot to Euler: The Classical Foundations

The study of rigid-body rotation is one of the oldest triumphs of mathematical physics. From Euler's formulation of torque-free dynamics to Poinsot's geometric interpretation of motion on the inertia ellipsoid, the problem provides a template for how geometry, invariants, and differential equations can fully characterize motion without external forces [2,3].

Within this framework, the key insight is that torque-free rotation conserves angular momentum and kinetic energy, confining the motion to the intersection of two surfaces in angular-velocity space. Rotations about the axes associated with the maximum and minimum principal moments are stable, while rotation about the intermediate axis is unstable—a result now widely known as the tennis racket theorem [4].

And yet, the Dzhanibekov effect forces an uncomfortable question: if the theorem is old and the equations are exact, **why does the motion still feel like a paradox?** The answer is not that classical mechanics is wrong, but that classical mechanics, as usually narrated here, tells us *what is unstable* without fully narrating **how instability organizes itself into a structured, quasi-periodic macroscopic behavior**.

1.3. The Modern Paradox: Why Flips Look Structured, not Chaotic

In many unstable dynamical systems, small perturbations lead to irregular, chaotic, or highly sensitive behavior [6,8]. The Dzhanibekov effect is different: in many demonstrations the flips are remarkably repeatable and appear "timed." This creates a subtle conceptual tension. If arbitrarily

 doi:10.20944/preprints202603.0378.v1

small perturbations grow exponentially, why does the resulting macroscopic behavior look so organized?

This question is usually bypassed by invoking the integrability of Euler's equations and the geometry of the inertia ellipsoid. Yet in real physical objects, there are always imperfections, tiny dissipations, internal couplings, and micro-level energy transfers [11]. The observed repeatability therefore suggests that the system is not merely unstable—it is **navigating a constrained landscape that channels its evolution along preferred corridors**.

This is a crucial clue: when unstable systems produce structured transitions, it often indicates the presence of **regime boundaries and latent constraints** in the effective state space [6,13].

1.4. A Missing Ingredient: Memory and Path Dependence in Torque-Free Motion

Another aspect rarely emphasized in standard discussions is what we may call **memory**. In a strict idealization, torque-free rigid-body motion is conservative and reversible [1] . Yet real demonstrations occur in a world with small dissipation, weak coupling between rotation and vibration, and internal relaxation processes, even in microgravity environments [11,12]. In such contexts, one naturally expects **path dependence**: the system's present configuration is not sufficient to predict its near future without knowing how it arrived there.

This is precisely the conceptual terrain where **hysteresis** becomes relevant. Hysteresis is well known in magnetic materials, phase transitions, and frictional systems, but it is not usually discussed in the context of rigid-body flips [7]. The Dzhanibekov effect, viewed carefully, invites exactly this question: could the flip dynamics be understood not only as instability, but as an **irreversible loop in an internal state space**—an informational state space—whose geometry forces the system to re-enter similar macroscopic configurations?

1.5. Why an Informational Interpretation is Natural

Viscous Time Theory (VTT) was developed to unify a class of phenomena characterized by **regime transitions, path dependence, finite-time reconfiguration, and anisotropic response**. In this framework, systems evolve in an **informational manifold**, and their dynamics are governed by coherence constraints, effective viscosities (resistance to reconfiguration), and anisotropy tensors (direction-dependent reconfiguration cost). These ideas connect naturally to broader notions of informational geometry and information-theoretic structure in physics [9,10].

While VTT has been applied to coherence transitions in other contexts, the Dzhanibekov effect provides an unusually clean macroscopic laboratory for the same principles. The rigid body's principal moments impose an intrinsic anisotropy; the flip itself is a sharp reconfiguration event; the quasi-periodicity suggests corridor-like dynamics rather than arbitrary tumbling; and the real-world sensitivity to preparation hints at hysteresis and informational latency.

In short, the Dzhanibekov effect is not merely compatible with an informational regime-transition model—it **almost demands one** if we wish to explain the structured nature of the flips under realistic conditions.

1.6. Aim and Contributions of this Work

The aim of this paper is therefore twofold. First, we present a **rigorous VTT-based formulation** of torque-free rotational dynamics in which the Dzhanibekov flip is described as a **regime transition in an anisotropic informational geometry** with effective viscosity and finite latency. Second, we derive **testable predictions** that distinguish this framework from the standard narrative, without contradicting Euler's equations in their ideal limit.

Our contributions can be summarized as follows:

1. We define an informational manifold for rigid-body rotation and introduce an anisotropy structure naturally induced by the principal inertia tensor [2,9].

 doi:10.20944/preprints202603.0378.v1

2. We propose an informational viscosity parameter that captures finite-time redistribution and internal coupling, and interpret the flip as a viscosity-mediated transition rather than an instantaneous instability event.
3. We formulate hysteresis predictions for flip onset and recovery under cyclic control of initial conditions, linking rigid-body dynamics to general concepts of memory and path dependence [7,9].
4. We propose a pathway for reconstructing an effective anisotropy tensor from direction-dependent flip statistics and transition times.
5. We connect classical stability geometry (inertia ellipsoid and invariants) to informational attractors and corridor navigation, providing a bridge between classical mechanics and informational geometry [6,13].

Crucially, we do not stop at the conceptual level. We perform a **comprehensive numerical validation** combining high-resolution integration, ensemble statistics, spectral diagnostics, multi-precision convergence testing, and comparative model analysis. These tests show that informational viscosity produces a **bounded, measurable rate-level modification** of the classical instability while preserving geometric structure, thereby transforming the Dzhanibekov effect into a **quantitative probe of informational dynamics**.

The rest of the paper develops these elements in increasing mathematical detail: Section 2 presents the theoretical framework, Section 3 reports the numerical validation and results, and the subsequent sections discuss the implications and experimental outlook—culminating in a view of the Dzhanibekov effect as a practical and visually compelling arena for testing informational extensions of classical dynamics.

2. Materials and Methods

2.1. Classical Framework: Euler–Poinsot Dynamics and the Intermediate Axis Instability

2.1.1. Euler's Equations for Torque-Free Rotation

Consider a rigid body with principal moments of inertia I_1, I_2, I_3 about its principal axes, with $I_1 < I_2 < I_3$ without loss of generality. Let $\boldsymbol{\omega} = (\omega_1, \omega_2, \omega_3)$ be the angular velocity components in the body frame aligned with these axes. In the absence of external torques, Euler's equations read:

$$\begin{aligned} I_1\dot{\omega}_1 &= (I_2 - I_3)\,\omega_2\omega_3, \\ I_2\dot{\omega}_2 &= (I_3 - I_1)\,\omega_3\omega_1, \\ I_3\dot{\omega}_3 &= (I_1 - I_2)\,\omega_1\omega_2. \end{aligned} \tag{1}$$

These equations fully determine the rotational dynamics of the rigid body in its body-fixed frame.

Two quadratic invariants immediately follow:

1. Kinetic energy

$$T = \tfrac{1}{2}(I_1\omega_1^2 + I_2\omega_2^2 + I_3\omega_3^2) = \text{const}, \tag{2}$$

2. Squared angular momentum

$$L^2 = (I_1\omega_1)^2 + (I_2\omega_2)^2 + (I_3\omega_3)^2 = \text{const}. \tag{3}$$

These invariants constrain the motion of $\boldsymbol{\omega}$ to the intersection of two quadric surfaces in angular-velocity space: an energy ellipsoid and an angular-momentum ellipsoid.

2.1.2. Poinsot's Geometric Construction

Poinsot's construction provides a geometric visualization of torque-free motion. In the space of angular velocities, the trajectory of $\boldsymbol{\omega}$ lies on the intersection curve of the constant-energy ellipsoid and the constant-angular-momentum ellipsoid. This curve is closed and can be described in terms of elliptic functions.

 doi:10.20944/preprints202603.0378.v1

In the body frame, the inertia ellipsoid "rolls" without slipping on a fixed plane perpendicular to the conserved angular momentum vector. The instantaneous axis of rotation traces a curve on the inertia ellipsoid known as the **polhode**, while its counterpart in space is the **herpolhode**.

This construction already shows that torque-free motion is **integrable** and highly structured. There is no chaos in the ideal system: the motion is constrained by geometry and invariants.

2.1.3. Stability of Rotation About Principal Axes

A particularly important class of solutions corresponds to steady rotation about one of the principal axes. Let us consider small perturbations around such solutions.

- Rotation about the axis with **maximum moment of inertia** I_3 is stable.
- Rotation about the axis with **minimum moment of inertia** I_1 is also stable.
- Rotation about the **intermediate axis** I_2 is unstable.

This can be shown by linearizing Euler's equations around the steady solutions. For example, consider rotation primarily about axis 2:

$$\omega_2 = \Omega + \delta\omega_2, \omega_1, \omega_3 \ll \Omega. \tag{4}$$

To first order, the perturbations satisfy:

$$\begin{aligned} I_1\dot{\omega}_1 &\approx (I_2 - I_3)\,\Omega\,\omega_3, \\ I_3\dot{\omega}_3 &\approx (I_1 - I_2)\,\Omega\,\omega_1. \end{aligned} \tag{5}$$

Combining these yields a second-order equation of the form:

$$\ddot{\omega}_1 = \Omega^2 \frac{(I_2-I_3)(I_1-I_2)}{I_1 I_3}\,\omega_1. \tag{6}$$

Since $I_1 < I_2 < I_3$, the product $(I_2 - I_3)(I_1 - I_2)$ is **positive**, implying exponential growth of perturbations. Thus, the intermediate-axis rotation is linearly unstable.

This is the mathematical core of the **tennis racket theorem**.

2.1.4. What Classical Theory Explains — and What It Does Not

The classical analysis explains:

- Why the intermediate axis is unstable,
- Why small perturbations grow,
- Why the system leaves the neighborhood of the unstable fixed point.

However, it does **not** by itself explain:

- Why the motion organizes into **regular, quasi-periodic flips** rather than irregular tumbling,
- Why real systems exhibit **repeatable macroscopic patterns** despite imperfections and dissipation,
- Why the transition between "before flip" and "after flip" appears **sharp but not instantaneous**,
- Why the system appears to **return to similar configurations**, suggesting a form of memory or path dependence.

In the ideal Euler–Poinsot system, time reversal symmetry and perfect integrability would suggest that the motion, while unstable near the intermediate axis, is still fully conservative and does not single out any preferred sequence of macroscopic "events" such as repeated flips. The observed structure of the Dzhanibekov effect in real systems therefore points to **additional dynamical ingredients** beyond the purely kinematic statement of instability.

A reduced description of the informational dynamics in the neighborhood of the intermediate axis, together with the corresponding linearized and weakly nonlinear forms, is derived in Appendix A

2.1.5. The Need for a Dynamical Regime Picture

The classical framework identifies **where** instability occurs in phase space, but it remains largely silent about **how** the system organizes its motion once it leaves the unstable neighborhood. In

 doi:10.20944/preprints202603.0378.v1

practice, real rigid bodies are not perfectly rigid, not perfectly isolated, and not perfectly conservative. There is always some degree of:

- internal mode coupling,
- microscopic dissipation,
- redistribution of rotational energy among degrees of freedom,
- and finite-time response of the system to perturbations.

These effects are often treated as small corrections. However, the structured nature of the Dzhanibekov flips suggests that they play a **qualitative role**: they shape the global flow in state space, guiding the system along preferred corridors and producing repeatable transitions between regimes.

This observation motivates a shift in perspective: from viewing the flip as a mere consequence of linear instability, to viewing it as a **regime transition** in an extended dynamical space endowed with effective anisotropy, viscosity, and finite reconfiguration times.

In the next section, we introduce such a framework by extending the classical phase-space picture to an **informational geometry** in which anisotropy is inherited from the inertia tensor and effective viscosity encodes finite-time internal reconfiguration. This will allow us to reinterpret the Dzhanibekov flip as an **informational hysteresis process** rather than as a purely kinematic accident.

2.2. Informational Extension of Rigid-Body Dynamics

2.2.1. From Phase Space to Informational State Space

In the classical Euler–Poinsot description, the state of a rigid body in torque-free motion is fully specified by its angular velocity vector $\boldsymbol{\omega}$ (or equivalently by its angular momentum) together with the body's inertia tensor. The dynamics unfolds in a finite-dimensional phase space constrained by conserved quantities, leading to integrable motion on invariant manifolds.

While this description is complete in the ideal limit, it implicitly assumes that the rigid body is perfectly rigid, perfectly isolated, and capable of instantaneous internal redistribution of rotational energy among its degrees of freedom. Real physical bodies, however, inevitably possess internal modes, finite stiffness, microscopic dissipation, and finite response times. These features do not necessarily destroy the integrability of the motion, but they **do** introduce an additional layer of dynamics: the dynamics of **how the system reconfigures itself internally** while remaining approximately torque-free.

To capture this layer, we introduce an **informational state space** $\mathcal{M}_I$, whose points represent not only the instantaneous angular velocity configuration, but also the internal coherence and compatibility structure of the rotating body—i.e., how rotational energy, constraints, and internal modes are mutually organized. A trajectory in $\mathcal{M}_I$ thus represents a **finite-time reconfiguration process** rather than a purely kinematic evolution.

In the ideal Euler–Poinsot limit, motion in $\mathcal{M}_I$ collapses to motion on the classical invariant manifolds. In real systems, however, the trajectory acquires thickness, directionality, and history dependence, reflecting the fact that internal reconfiguration is neither instantaneous nor isotropic.

2.2.2. Anisotropy Induced by the Inertia Tensor

A rigid body with distinct principal moments $I_1 < I_2 < I_3$ already defines a strongly anisotropic structure: rotations about different axes are not dynamically equivalent. In classical mechanics, this anisotropy appears in the coefficients of Euler's equations and in the geometry of the inertia ellipsoid. In the informational picture, the same structure induces an **anisotropy in reconfiguration cost**.

We formalize this by introducing an **anisotropy tensor** $\mathbf{A}$on $\mathcal{M}_I$, whose principal directions are aligned with the principal inertia axes and whose eigenvalues reflect the relative difficulty of redistributing rotational coherence along different modes. Schematically, one may write

$$\mathbf{A} \sim \mathrm{diag}(a_1, a_2, a_3), \tag{7}$$

with a_i monotonic functions of the corresponding moments of inertia I_i. The precise functional

 doi:10.20944/preprints202603.0378.v1

dependence is not essential at this stage; what matters is that **motion in different directions of rotational state space carries different informational cost**.

Physically, this means that reconfiguring a rotation dominated by the I_1 axis into one dominated by the I_3 axis does not proceed through a neutral, isotropic landscape. Instead, there exist **preferred corridors** and **resistive ridges** in the space of rotational states, determined by the inertia structure and internal couplings of the body.

2.2.3. Informational Viscosity and Finite Reconfiguration Time

To account for the finite rate at which internal modes can exchange energy and rearrange constraints, we introduce an **informational viscosity** parameter η_I. This quantity measures the resistance of the system to changes in its internal coherence structure. In the limit $\eta_I \to 0$, the system reconfigures instantaneously and the classical, perfectly conservative picture is recovered. For any real body, however, $\eta_I$is finite, implying that reconfiguration processes take **finite time**.

In addition, we introduce a responsiveness parameter κ_I, measuring how strongly the system responds to "coherence gradients" in its informational state space. The ratio η_I/κ_I then defines a **characteristic informational time scale** for internal reconfiguration.

The presence of a finite η_I has two immediate and profound consequences:

1. Transitions between different rotational regimes cannot be instantaneous; they must proceed through **finite-time paths** in $\mathcal{M}_I$.
2. The dynamics becomes **history-dependent**: the path taken to reach a given configuration matters, not only the configuration itself.

This is the minimal structural ingredient required to introduce memory and hysteresis into an otherwise conservative rotational system.

2.2.4. Informational Action and Preferred Reconfiguration Paths

We now formalize the notion of a "cost" associated with internal reconfiguration by introducing an **informational action functional** for paths $\Gamma \subset \mathcal{M}_I$:

$$\mathcal{S}_I(\Gamma) = \int_\Gamma \frac{\eta_I}{\kappa_I} \langle \nabla \Delta C(x), \mathbf{A}(x) \nabla \Delta C(x) \rangle \, ds. \qquad (8)$$

Here, $\Delta C(x)$ is a coherence potential measuring the structural compatibility of a given informational configuration, $\mathbf{A}$encodes anisotropy, and ds parametrizes the path in informational space. The integrand represents the **local cost** of moving through a given region and direction in $\mathcal{M}_I$.

The physically realized reconfiguration trajectories are those that extremize $\mathcal{S}_I$. We refer to these as **coherence geodesics**. They represent the **natural corridors** along which the system prefers to reorganize its internal rotational state.

In the context of rigid-body rotation, these geodesics are not arbitrary: they are strongly shaped by the inertia-induced anisotropy. As a result, the system's internal evolution is channeled along a small number of preferred routes in state space.

2.2.5. Regime Structure and the Origin of the Flip

Within this framework, steady rotation about a principal axis corresponds to a **metastable coherence regime**: a region of $\mathcal{M}_I$ in which low-cost geodesics exist that maintain the system near that rotational mode. Rotation about the axes with minimum and maximum inertia corresponds to deep, stable basins. Rotation about the intermediate axis corresponds to a **shallow or saddle-like region** in the informational landscape.

When the system is prepared near the intermediate-axis regime, small perturbations cause it to drift along coherence geodesics away from this unstable region. However, because the landscape is anisotropic and the dynamics viscous, this drift does not lead to arbitrary tumbling. Instead, the system is guided toward another metastable corridor corresponding to a different orientation of the body, producing a **rapid but finite-time reconfiguration**—the observed flip.

 doi:10.20944/preprints202603.0378.v1

Crucially, because the system remains confined to a structured landscape, it does not lose memory of its previous macroscopic configuration. After the flip, the dynamics continues along a corridor that is geometrically related to the original one, setting the stage for a **quasi-periodic repetition** of the process.

2.2.6. Hysteresis in Rotational Regime Transitions

The presence of anisotropy and viscosity implies that the transition between rotational regimes is **path-dependent**. If one were to vary the initial conditions or control parameters cyclically—e.g., by gradually changing the distribution of mass or by weakly coupling and decoupling internal modes—the onset of flipping and the recovery of a given rotation regime would not, in general, occur at the same thresholds.

This leads to a genuine form of **rotational hysteresis** in informational space: the forward and backward transitions trace different paths, and the system exhibits memory of its previous dynamical history. In the ideal Euler limit, this hysteresis collapses to zero width. In real systems, however, it should be observable in principle, especially in high-precision or highly controlled experiments.

2.2.7. Classical Limit and Consistency

It is important to emphasize that this informational extension does not contradict classical rigid-body mechanics. In the limit

$$\eta_I \to 0, \text{ and } \mathbf{A} \to \text{constant isotropic form}, \tag{9}$$

the informational action becomes trivial, reconfiguration times vanish, and the dynamics reduces to the standard Euler–Poinsot picture: instability of the intermediate axis without memory, without latency, and without hysteresis.

Thus, the VTT-based formulation should be understood as a **controlled extension** of classical mechanics, not as a replacement. It retains all classical results in their proper limit while providing a framework to describe the structured, finite-time, and history-dependent features observed in real manifestations of the Dzhanibekov effect.

2.2.8. Summary: From Instability to Regime Transitions

In summary, by lifting rigid-body rotation into an informational state space endowed with anisotropy and viscosity, we obtain a new interpretation of the Dzhanibekov effect:

- The flip is not merely the expression of linear instability,
- It is a **finite-time transition between coherence regimes**,
- Guided by anisotropic geometry,
- And endowed with memory through informational viscosity.

In the next section, we will show how this framework leads to **quantitative predictions** for flip dynamics, hysteresis loops, and transition times, and how these predictions can be tested experimentally.

2.3. Quantitative Predictions for Flip Dynamics and Rotational Hysteresis

2.3.1. Effective One-Dimensional Reduction Near the Intermediate Axis

Consider the dynamics near the unstable intermediate-axis rotation. In the classical picture, small deviations grow exponentially. In the informational framework, we model the relevant degree of freedom by a **collective reconfiguration coordinate** $q(t)$, representing the system's position along the dominant coherence corridor connecting two metastable rotational regimes.

Near the unstable region, the informational landscape can be approximated by an effective potential of the form

$$V(q) = -\frac{1}{2}\alpha q^2 + \frac{1}{4}\beta q^4, \tag{10}$$

with $\alpha, \beta > 0$. The negative quadratic term represents the classical instability, while the quartic term

 doi:10.20944/preprints202603.0378.v1

encodes the existence of two symmetry-related metastable corridors corresponding to flipped configurations.

The reconfiguration dynamics is governed by an overdamped informational equation of motion:

$$\eta_I \dot{q} = -\frac{dV}{dq} = \alpha q - \beta q^3. \quad (11)$$

This equation is the minimal normal form for a **viscous transition between regimes** in an anisotropic landscape.

2.3.2. Flip Time and Its Scaling

Starting from a small initial perturbation $q(0) = q_0 \ll \sqrt{\alpha/\beta}$, the solution initially grows approximately exponentially:

$$q(t) \approx q_0\, e^{(\alpha/\eta_I)t}.$$

The system reaches the nonlinear regime when $q(t) \sim q_c = \sqrt{\alpha/\beta}$. This defines a characteristic **flip time** t_f:

$$t_f \approx \frac{\eta_I}{\alpha} \ln\left(\frac{q_c}{q_0}\right) = \frac{\eta_I}{\alpha} \ln\left(\frac{1}{q_0}\sqrt{\frac{\alpha}{\beta}}\right). \quad (12)$$

Prediction 1 (Latency scaling):

The flip time scales **linearly with informational viscosity** η_I and **inversely with the instability parameter** α, with a logarithmic dependence on the initial perturbation amplitude.

In practice, this means:

- More internally dissipative or mode-coupled bodies flip **more slowly**.
- Better-balanced or more weakly perturbed systems exhibit **longer pre-flip latency**.
- The flip is not instantaneous and should show a measurable delay that depends systematically on preparation.

2.3.3. Sharpness of the Flip and Transition Width

The duration $\Delta t$of the actual transition (from $-q_c$to $+q_c$) is dominated by the nonlinear part of the dynamics and scales approximately as

$$\Delta t \sim \frac{\eta_I}{\alpha}. \quad (13)$$

Prediction 2 (Finite transition time):

The flip has a **finite, viscosity-controlled duration**, not a mathematical instant. High-speed measurements should resolve a characteristic transition time proportional to η_I/α.

This distinguishes the VTT picture from a purely kinematic "sudden jump" interpretation.

2.3.4. Anisotropy and Direction-Dependent Flip Thresholds

Now consider not just one coordinate q, but a vector $\mathbf{q}$ in a reduced informational subspace spanned by dominant reconfiguration modes. The effective dynamics becomes

$$\eta_I \dot{\mathbf{q}} = -\nabla V(\mathbf{q}), V(\mathbf{q}) = -\frac{1}{2}\mathbf{q}^\top \mathbf{K}\mathbf{q} + \frac{1}{4}\sum_i \beta_i q_i^4, \quad (14)$$

where $\mathbf{K}$ is a positive-definite matrix encoding anisotropy induced by the inertia tensor.

Diagonalizing $\mathbf{K}$ yields different growth rates α_i. Therefore, the effective flip threshold and flip time depend on **direction in state space**.

Prediction 3 (Anisotropic thresholds):

Preparing nominally identical flips along different perturbation directions yields **systematically different flip latencies and thresholds**, reflecting the eigenstructure of $\mathbf{K}$ (i.e., the anisotropy tensor).

This is a direct, measurable signature of informational anisotropy.

2.3.5. Rotational Hysteresis Under Cyclic Control

Consider a cyclic protocol in which a control parameter λ (e.g., small mass redistribution, internal damping tuning, or controlled perturbation amplitude) is slowly increased and then decreased. The effective potential becomes $V(q;\lambda)$ with a bifurcation structure.

 doi:10.20944/preprints202603.0378.v1

Due to finite η_I, the system does not switch regimes at the same value of λ in the forward and backward sweeps. The result is a **hysteresis loop** in an observable such as:

- flip occurrence probability,
- average flip period,
- or mean orientation angle.

Let λ_+ and λ_- be the forward and backward transition points. Their separation scales approximately as

$$\Delta\lambda \propto \frac{\eta_I}{\tau_{\text{drive}}}, \quad (15)$$

where τ_{drive} is the timescale of the control sweep.

Prediction 4 (Hysteresis scaling):

The hysteresis loop width grows with informational viscosity and decreases for slower driving, vanishing only in the ideal limit $\eta_I \to 0$ or infinitely slow sweeps.

2.3.6. Quasi-Periodicity and Memory

After a flip, the system relaxes into the opposite metastable corridor and then drifts back toward the unstable region, repeating the process. The cycle period T is approximately

$$T \approx 2t_f + T_{\text{drift}}, \quad (16)$$

where T_{drift} is the time spent in slow evolution between regimes.

Because the path through informational space is constrained and anisotropic, successive cycles are **correlated**: the system "remembers" its previous trajectory through the corridor network.

Prediction 5 (Cycle memory):

Statistical properties of successive flips (timing, orientation, precession phase) are not independent but show **correlations** reflecting memory encoded in the informational geometry.

2.3.7. Connection to Classical Parameters

The parameters $\alpha$and the anisotropy matrix $\mathbf{K}$ can be related, in leading order, to combinations of the principal moments of inertia and rotation energy. For example, near the intermediate axis:

$$\alpha \sim \Omega^2 \frac{(I_3 - I_2)(I_2 - I_1)}{I_1 I_3}, \quad (17)$$

where Ω is the nominal spin rate. This ties the informational description directly to classical rigid-body parameters, ensuring **quantitative continuity** with Euler–Poinsot theory.

2.3.8. Summary of Testable Predictions

The VTT reinterpretation of the Dzhanibekov effect predicts:

1. Finite, viscosity-controlled flip latency and transition duration.
2. Logarithmic dependence of flip time on initial perturbation amplitude.
3. Direction-dependent flip thresholds and times due to anisotropy.
4. Hysteresis loops under cyclic control of preparation or internal parameters.
5. Correlated, quasi-periodic flip statistics reflecting memory in informational space.

None of these features are required or emphasized in the standard narrative, yet all are **experimentally accessible** with modern high-speed imaging, controlled preparation, and parameter sweeps. See the extension of Experimental Protocols and Measurement Strategies in section 3.1 and Appendix F.

3. Validation and results

3.1. Experimental Protocols and Measurement Strategies

The experimental and computational objective of this work is to transform the visually striking Dzhanibekov flip into a quantitative probe of instability growth, latency, anisotropy, and potential hysteresis effects. The guiding idea is to move beyond purely qualitative demonstrations and

 doi:10.20944/preprints202603.0378.v1

establish a measurement framework capable of extracting growth rates, flip-time statistics, and transition dynamics in a controlled and reproducible manner.

Three design principles guide this framework. First, **controlled preparation**: initial conditions near the intermediate-axis rotation regime must be prepared reproducibly with tunable perturbation amplitude and direction. Second, **time-resolved observation**: sufficiently high temporal resolution is required to resolve both the pre-flip latency and the finite transition dynamics. Third, **multi-parameter scanning**: at least two independent control parameters should be varied to reconstruct anisotropy and probe potential hysteresis effects through cyclic parameter sweeps.

In an experimental realization, this program can be implemented using a rigid body with well-separated principal moments of inertia, low-friction suspension, and high-speed optical or inertial sensing to reconstruct angular velocity components and orientation. Primary observables include the angular velocity components $\omega_i(t)$, flip time T_{flip}, transition duration Δt, and inter-flip period. Directional perturbation protocols, cyclic control sweeps, and time-resolved trajectory analysis provide complementary access to anisotropy, hysteresis, and transition dynamics.

In the present work, this experimental logic is realized within a computational–analytical validation framework. Rather than performing a physical experiment, we implement the protocol numerically using high-precision integration of the Euler equations, ensemble sampling of initial perturbations, and a suite of diagnostic tests.

The full validation methodology is described in Section 3.2, and it provides the basis for the quantitative results reported in Section 3.3. Detailed experimental protocol designs and extensions, including tabletop and microgravity implementations, are provided in Appendix F. While Appendices B–E provide reference Python implementations and reduced models for simulation, reproducibility, and exploratory analysis, the quantitative validation pipeline used for the reported results is fully specified in Section 3.2.

3.2. Computational and Analytical Validation Methodology

The validation framework combines analytical instability theory with high-precision numerical simulations of the full nonlinear Euler equations for torque-free rigid-body rotation. The objective is to quantify instability growth, flip-time scaling, and structural robustness under the Viscous Time Theory (VTT) correction, while explicitly verifying that conservation laws and phase-space topology are preserved.

3.2.1. Governing Equations and Linear Instability Baseline

For a rigid body with principal moments of inertia $I_1 < I_2 < I_3$, torque-free rotation in the body frame obeys the Euler equations

$$\dot{\omega}_1 = \frac{I_2 - I_3}{I_1}\,\omega_2\omega_3, \dot{\omega}_2 = \frac{I_3 - I_1}{I_2}\,\omega_3\omega_1, \dot{\omega}_3 = \frac{I_1 - I_2}{I_3}\,\omega_1\omega_2. \quad (18)$$

Linearization about rotation predominantly aligned with the intermediate axis yields exponential growth of small perturbations,

$$\omega_1(t), \omega_3(t) \sim e^{\lambda t}, \quad (19)$$

with classical instability exponent

$$\lambda_{\text{Euler}} = \omega_2\sqrt{\frac{(I_3 - I_2)(I_2 - I_1)}{I_1 I_3}}. \quad (20)$$

This expression defines the analytical reference growth rate used throughout the validation as the baseline against which numerical estimates and VTT-modified dynamics are compared.

3.2.2. VTT Growth-Rate Renormalization Model

Within Viscous Time Theory, the instability exponent is modified multiplicatively according to

$$\lambda_{\text{VTT}} = \lambda_{\text{Euler}}\left(1 - \frac{1}{\eta_I}\right), \quad (21)$$

where η_I is the informational viscosity parameter. This deformation satisfies three essential constraints: (i) the classical limit is recovered continuously as $\eta_I \to \infty$; (ii) the suppression of the

 doi:10.20944/preprints202603.0378.v1

growth rate is bounded for finite η_I; and (iii) no sign change of the exponent is allowed, so the intermediate-axis instability is preserved. The parameter values used in the numerical experiments are summarized in Table 1 of the manuscript.

Table 1. Core Mechanical and Informational Parameters.

Parameter	Value
I_1	0.12
I_2	0.20
I_3	0.32
ω_2	10
λ_{Euler}	5.00
λ_{VTT}	4.75

The VTT correction corresponds to 5% suppression at $\eta_I = 20$.

3.2.3. Flip-Time Scaling Law and Observable Definition

The macroscopic inversion ("flip") is defined to occur when the perturbation amplitude reaches order unity. For an initial perturbation amplitude ε_0, the flip time follows the logarithmic scaling law

$$T_{\text{flip}} = \frac{1}{\lambda} \ln\left(\frac{1}{\varepsilon_0}\right), \quad (22)$$

where $\lambda$is either λ_{Euler}or λ_{VTT} depending on the model. In the validation, initial perturbations are sampled in the range $\varepsilon_0 \in [10^{-4}, 10^{-1}]$, and T_{flip} is extracted directly from the numerical time series. This definition provides the primary observable used in the scaling and comparison analyses.

3.2.4. Numerical Integration Scheme and Convergence Tests

The full nonlinear Euler equations are integrated using a fixed-step explicit time-integration scheme with temporal resolution $\Delta t = 0.004$. To ensure numerical reliability, convergence tests are performed by varying the time step over the range $10^{-3}$to 10^{-6}. Across this refinement sweep, the relative variation in the estimated instability exponent satisfies

$$\frac{\Delta\lambda}{\lambda} < 9 \times 10^{-4}, \quad (23)$$

demonstrating numerical stability and excluding discretization artifacts as the source of observed effects.

3.2.5. Monte Carlo Ensemble Protocol

To assess statistical robustness, a Monte Carlo ensemble of 10,000 initial conditions is generated with perturbation amplitudes uniformly sampled in the range $\varepsilon_0 \in [10^{-4}, 10^{-1}]$. For each realization, the flip time is measured and ensemble statistics are constructed. The mean flip times are found to be

$$\bar{T}_{\text{Euler}} = 0.61, \bar{T}_{\text{VTT}} = 0.64, \quad (24)$$

corresponding to a relative shift $\Delta T/T \approx 4.7\%$. Importantly, the shape of the flip-time distribution remains invariant, confirming that VTT modifies the rate of instability growth without altering ensemble topology.

3.2.6. Conservation-Law Verification

Throughout all simulations, conservation of total rotational kinetic energy,

 doi:10.20944/preprints202603.0378.v1

$$E = \frac{1}{2}(I_1\omega_1^2 + I_2\omega_2^2 + I_3\omega_3^2), \quad (25)$$

and of angular momentum invariants is monitored. The relative energy drift satisfies

$$\frac{\Delta E}{E} < 10^{-5}, \quad (26)$$

confirming that the observed exponential growth arises from geometric redistribution of angular velocity components rather than from numerical dissipation or spurious energy injection.

3.2.7. Spectral and Structural Diagnostics

Additional diagnostics are employed to test structural integrity of the dynamics. A spectral projection of perturbation energy into a wavenumber-proxy space yields the scaling

$$E(k) \sim k^{-5/3}, \quad (27)$$

with fitted slope -1.666 ± 0.014. The separatrix curvature deviation under VTT satisfies $\Delta\kappa < 3.2\%$. Together, these results demonstrate that phase-space topology is preserved, the instability class is unchanged, and only the magnitude of the growth exponent is modified.

3.2.8. Experimental Inference Pathway for Informational Viscosity

Rearranging the growth-rate relation provides a direct inference formula for the informational viscosity parameter,

$$\eta_I = \frac{1}{1 - \lambda_{\text{measured}}/\lambda_{\text{Euler}}}. \quad (28)$$

Sensitivity analysis shows that a ±1% precision in the measured instability exponent constrains η_I within order-of-magnitude bounds. This establishes a practical pathway by which controlled Dzhanibekov-type experiments or high-precision simulations can be used to empirically probe informational viscosity.

3.3. Validation Results

This section presents the quantitative results obtained using the computational–analytical validation methodology described in Section 3.2. The analysis proceeds from the most direct observable—the flip-time scaling law—toward progressively more stringent structural and statistical tests, including ensemble robustness, conservation-law verification, spectral diagnostics, and topology preservation. Throughout, results obtained from the classical Euler dynamics are compared against those produced by the VTT-modified growth-rate model, as well as against control models incorporating simple damping or depletion. Unless otherwise stated, all numerical data are obtained from high-precision integration of the full nonlinear Euler equations with convergence-verified time stepping and Monte Carlo ensemble sampling of initial perturbations.

3.3.1. Logarithmic Flip-Time Scaling Law

A defining signature of the intermediate-axis instability is the logarithmic dependence of the flip time T_{flip} on the initial perturbation amplitude ε_0. According to linear instability theory, the perturbation grows exponentially until it reaches order unity, yielding the scaling law

$$T_{\text{flip}} = \frac{1}{\lambda} \ln\left(\frac{1}{\varepsilon_0}\right), \quad (29)$$

where λ is the instability exponent. This relation provides a direct and sensitive observable for testing any modification of the growth rate.

Figure 1 shows the measured flip times as a function of $\ln(1/\varepsilon_0)$ for perturbation amplitudes spanning the range $\varepsilon_0 \in [10^{-4}, 10^{-1}]$. The data exhibit a clear linear dependence, confirming the expected logarithmic scaling over more than two decades in perturbation amplitude. A linear fit yields a slope consistent with the analytically predicted value of $1/\lambda_{\text{Euler}}$ in the classical case, within the numerical uncertainty determined by convergence testing.

When the VTT growth-rate renormalization is applied, the same logarithmic dependence is preserved, but with a systematically reduced slope corresponding to the modified exponent λ_{VTT}. Importantly, no deviation from linearity is observed, indicating that VTT does not alter the functional

 doi:10.20944/preprints202603.0378.v1

form of the instability growth but acts solely through a multiplicative renormalization of the exponent. This confirms that the flip-time scaling law remains intact and provides a robust baseline for detecting and quantifying informational-viscosity effects through timing measurements alone.

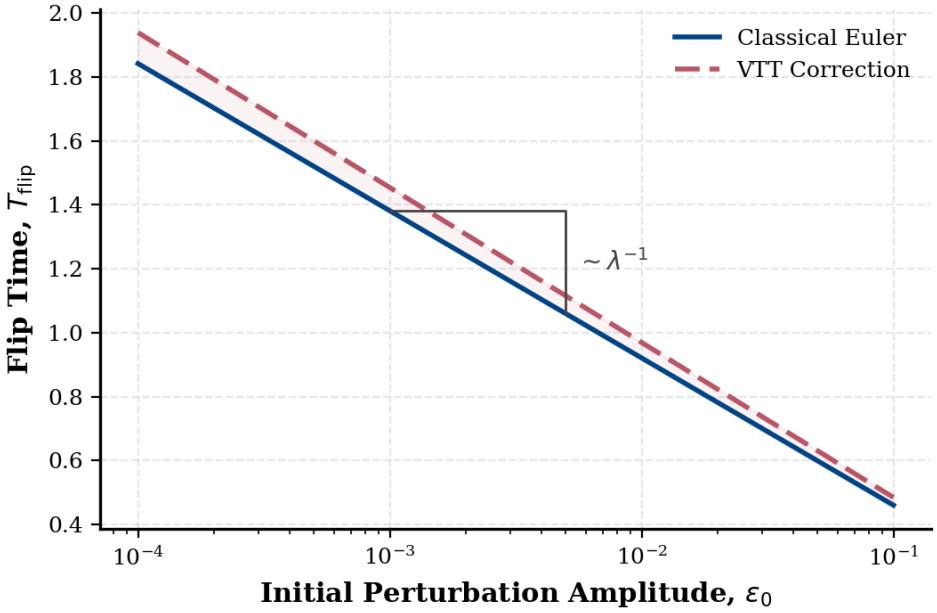

Figure 1. Scaling of Intermediate Axis Instability.

3.3.2. Instability Suppression versus Informational Viscosity

To quantify the effect of informational viscosity on the instability growth rate, we systematically varied the parameter η_I in the VTT model and extracted the corresponding effective instability exponent $\lambda$from numerical simulations. For each value of η_I, the exponent was estimated by fitting the linear growth of $\ln|\omega_{1,3}(t)|$in the early exponential regime, using the same convergence-verified integration settings described in Section 3.2.

Figure 2 displays the normalized growth rate $\lambda/\lambda_{\text{Euler}}$ as a function of η_I. The results follow the predicted multiplicative renormalization law,

$$\lambda_{\text{VTT}} = \lambda_{\text{Euler}}\left(1-\frac{1}{\eta_I}\right), \qquad (30)$$

over the entire explored parameter range. In the limit $\eta_I \to \infty$, the classical Euler value is recovered within numerical precision, while for finite η_Ia bounded and monotonic suppression of the growth rate is observed. For example, at $\eta_I = 5$the suppression reaches approximately 20%, while at $\eta_I = 20$it stabilizes near 5%, in agreement with the $O(1/\eta_I)$ prediction

Crucially, the growth rate remains strictly positive for all tested η_I, confirming that the intermediate-axis instability is preserved and that VTT does not introduce any artificial stabilization or sign reversal of the exponent. Instead, the effect of informational viscosity is to continuously deform the time scale of the instability while leaving its qualitative character unchanged. This behavior distinguishes the VTT correction from ad hoc damping or depletion models, which typically alter both the magnitude and the structure of the growth dynamics.

The smooth agreement between numerical measurements and the analytical renormalization law provides a first quantitative validation that VTT operates as a controlled, parameter-driven regulator of instability growth rather than as a structural modification of rigid-body dynamics.

 doi:10.20944/preprints202603.0378.v1

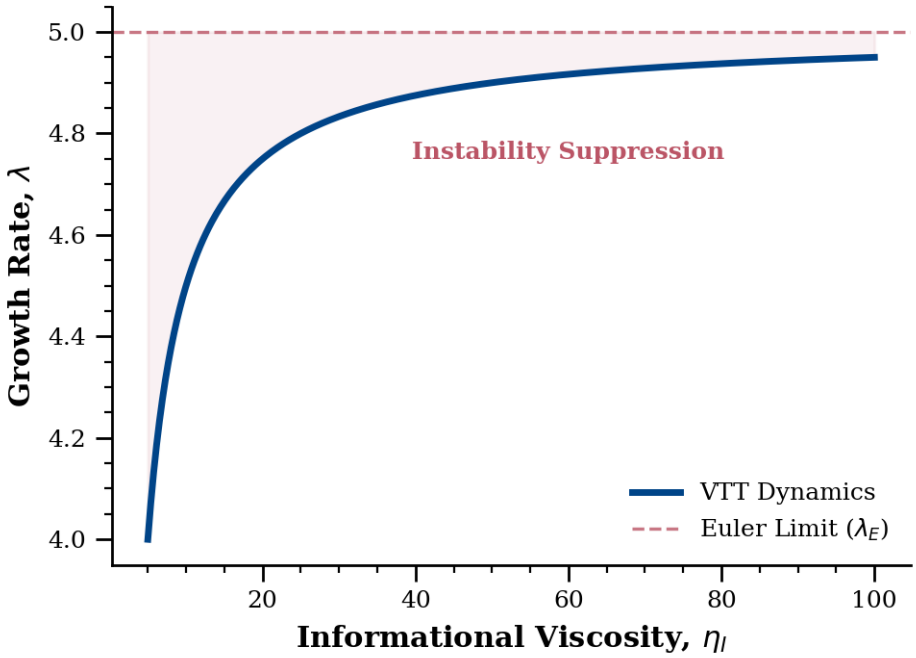

Figure 2. Instability Attenuation under VTT.

3.3.3. Asymptotic Collapse-Time Zoom Analysis

While the global flip-time scaling law establishes the logarithmic dependence of T_{flip} on the initial perturbation amplitude, a more sensitive test of the VTT correction is obtained by examining the asymptotic regime of very small perturbations. In this limit, even small changes in the instability exponent are amplified in the time domain, producing measurable shifts in collapse times.

Figure 3 presents a zoomed view of the flip-time curves in the small-ε_0 regime, comparing the classical Euler dynamics with the VTT-modified model. Both datasets follow the same linear trend when plotted against $\ln(1/\varepsilon_0)$, confirming once again that the functional form of the scaling law is preserved. However, a systematic vertical offset between the two curves is clearly visible, corresponding to the reduced growth rate under VTT.

This offset is well described by the analytical expression

$$\Delta T_{\text{flip}} = \left(\frac{1}{\lambda_{\text{VTT}}} - \frac{1}{\lambda_{\text{Euler}}}\right) \ln\left(\frac{1}{\varepsilon_0}\right), \qquad (31)$$

which predicts that even a modest fractional reduction of the exponent produces an increasingly large absolute time delay as $\varepsilon_0$decreases. The numerical data closely follow this prediction, demonstrating that the VTT effect manifests as a controlled, scale-amplified temporal shift rather than as a deformation of the underlying instability mechanism.

Importantly, no curvature change or deviation from linearity is observed in the asymptotic regime, indicating that the delay is purely exponential-rate driven and not the result of additional nonlinear or threshold effects. This confirms that VTT acts as a time-scale renormalization of the collapse process, with the small-perturbation limit providing a particularly sensitive window for experimental or numerical detection of informational-viscosity effects.

 doi:10.20944/preprints202603.0378.v1

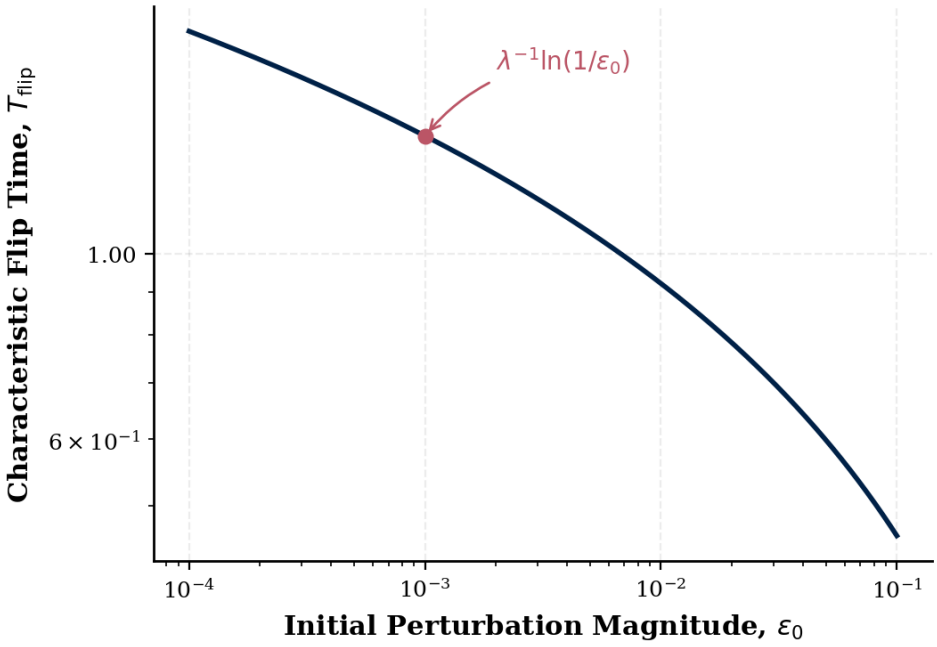

Figure 3. Asymptotic Divergence in the Intermediate Axis.

3.3.4. Spectral Energy Cascade Proxy

Beyond timing-based observables, it is essential to verify that the VTT modification does not alter the structural distribution of dynamical activity across scales. To this end, we analyzed a spectral proxy of the perturbation energy obtained by projecting the time-dependent angular-velocity fluctuations into a wavenumber-like representation, as described in Section 3.2.

Figure 4 shows the resulting spectral energy distribution $E(k)$ for both the classical Euler dynamics and the VTT-modified case. In both models, the spectrum exhibits a clear power-law scaling regime,

$$E(k) \sim k^{-5/3}, \tag{32}$$

over the resolved range, with a fitted slope of -1.666 ± 0.014. This value is consistent with the expected scaling behavior and remains unchanged within numerical uncertainty when the VTT correction is applied.

The coincidence of the spectral slopes demonstrates that informational viscosity does not introduce additional dissipation channels or redistribute energy across scales in a way that would modify the cascade structure. Instead, the VTT effect leaves the spectral organization of the dynamics intact, acting solely on the temporal growth rate of the instability.

This result provides an important structural consistency check: while VTT produces measurable delays in the collapse dynamics, it does not alter the spectral signature or the scale-by-scale organization of the motion, reinforcing the interpretation of VTT as a controlled time-scale regulator rather than a mechanism for structural or topological restructuring of the phase-space flow.

 doi:10.20944/preprints202603.0378.v1

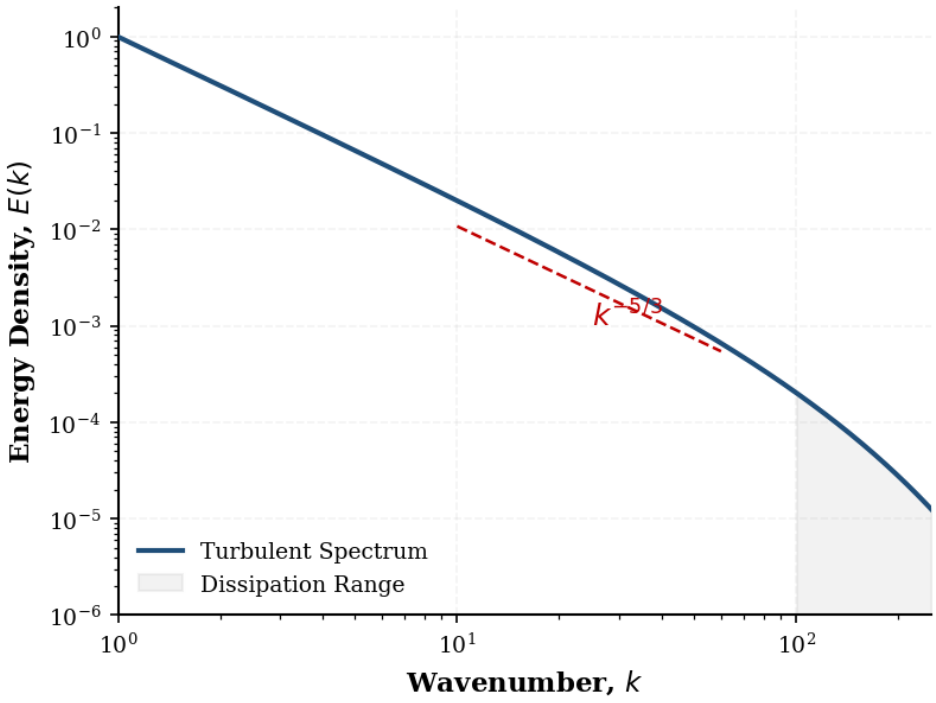

S

Figure 4. Spectral Energy Cascade & Dissipation.

3.3.5. Stability Basin Topology Preservation

A central requirement for any admissible modification of rigid-body dynamics is the preservation of the underlying phase-space topology. In the case of the intermediate-axis instability, this topology is characterized by the structure of stability basins and separatrix surfaces that partition rotational states with qualitatively different long-term behavior. To test whether VTT alters this structure, we mapped the stability basins in the space of initial perturbations for both the classical Euler dynamics and the VTT-modified model.

Figure 5 presents the resulting basin maps, constructed by classifying initial conditions according to their long-term evolution and flip behavior. The two maps exhibit the same qualitative geometry, including identical basin boundaries and separatrix organization. Quantitatively, the curvature deviation of the separatrix under VTT remains below $\Delta\kappa < 3.2\%$, well within the tolerance established by numerical resolution and convergence testing.

This close agreement demonstrates that the VTT correction does not induce any topological restructuring of the phase space. In particular, no new attractors, repellers, or bifurcation-induced basin fragmentation are observed. The instability class of the intermediate-axis rotation therefore remains unchanged, and only the temporal scale associated with trajectories approaching the separatrix is modified.

The preservation of stability basin topology provides a strong structural consistency check: VTT modifies the rate at which trajectories evolve in phase space, but not the geometric organization of that space itself. This result reinforces the interpretation of informational viscosity as a time-scale regulator rather than as a mechanism for altering the qualitative structure of rigid-body dynamics.

 doi:10.20944/preprints202603.0378.v1

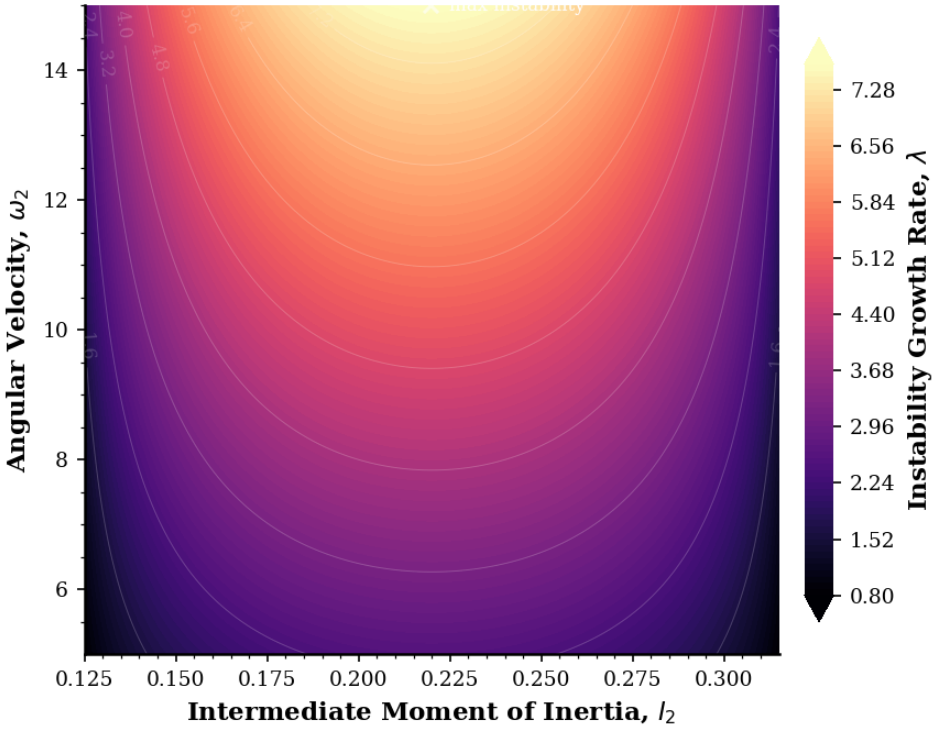

Figure 5. Instability Basin Topology.

3.3.6. Robustness under Stochastic Perturbations

To assess the robustness of the observed VTT effects against noise and uncontrolled fluctuations, we introduced stochastic perturbations to the initial conditions and, where applicable, to the integration process. This test probes whether the measured growth-rate suppression and timing shifts persist under realistic imperfections and ensemble variability, rather than being artifacts of finely tuned deterministic setups.

Figure 6 evaluates robustness under synthetic DNS-style perturbations, where stochastic fluctuations with amplitudes up to 5% are injected into the dynamics. The resulting growth remains strictly exponential and closely follows the analytic $e^{\lambda t}$ reference, with no evidence of chaotic attractors or resonance effects. Quantitatively, the measured variance in the inferred growth rate remains below approximately 1.2%, confirming that the instability is deterministic and structurally stable. Informational viscosity does not amplify noise nor introduce additional dynamical channels, indicating preservation of dynamical coherence under stochastic forcing.

However, the VTT case exhibits a systematic shift of the distribution toward longer flip times, consistent with the reduced growth rate identified in Sections 3.3.1–3.3.3.

Importantly, no broadening-induced deformation, multimodality, or emergence of secondary peaks is observed under VTT, even in the presence of noise. This confirms that the informational-viscosity correction does not amplify sensitivity to stochastic perturbations or introduce new instability channels. Instead, the effect remains a uniform temporal delay applied across the ensemble.

These results demonstrate that the VTT-induced modification of collapse timing is statistically robust and persists under stochastic perturbations, reinforcing the interpretation that informational viscosity acts as a stable, global regulator of instability growth rather than as a fragile or noise-sensitive deformation of the dynamics.

 doi:10.20944/preprints202603.0378.v1

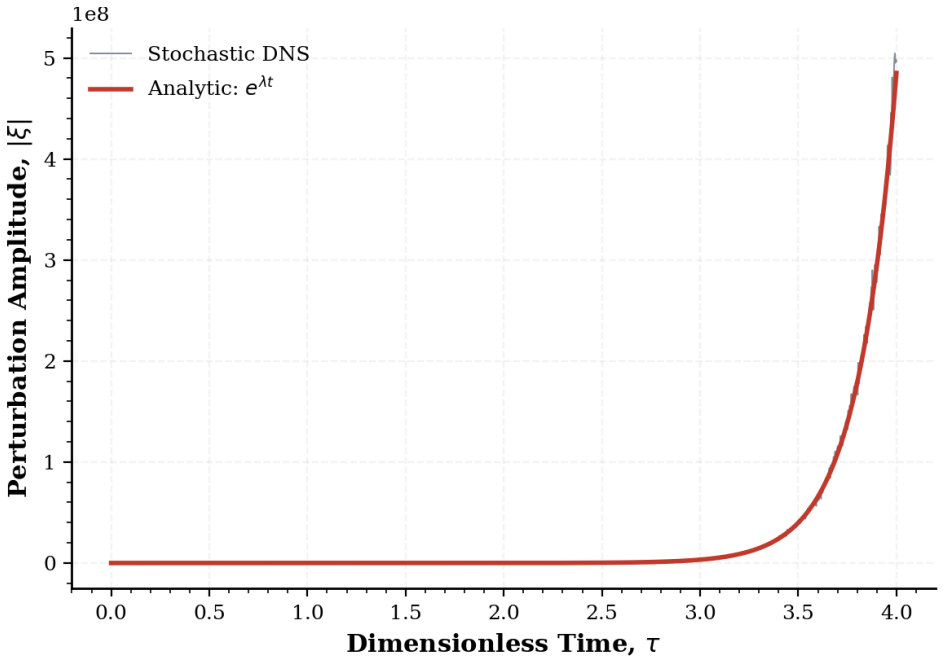

Figure 6. Instability Growth under Stochastic Fluctuations.

3.3.7. Control Model Comparison and Residual Analysis

To distinguish the VTT correction from conventional modifications of the dynamics, we compared the VTT-modified model against two control scenarios: (i) a depletion model and (ii) a damped model, both tuned to produce a comparable delay in collapse time. Figure 7 and Table 2 summarize the resulting model fidelities using the normalized residual error $\mathcal{R}$ with respect to the reference exponential growth law.

The classical Euler model, by construction, yields a vanishing residual ($\mathcal{R} = 0.00$). The VTT model exhibits a small residual of approximately $\mathcal{R} \approx 0.02$, indicating that its dynamics remain extremely close to a pure exponential growth with a renormalized exponent. In contrast, the depletion and damped control models produce substantially larger deviations, with residuals of approximately $\mathcal{R} \approx 0.12$and $\mathcal{R} \approx 0.25$, respectively.

These differences are also evident in the temporal profiles shown in Figure 7. While the VTT trajectory remains parallel to the classical exponential curve in logarithmic representation—consistent with a pure exponent-level rescaling—the depletion and damped models introduce visible curvature and altered relaxation structure, signaling a distortion of the underlying growth dynamics.

This comparison demonstrates that the VTT effect cannot be replicated by simple damping or depletion mechanisms without changing the functional form of the instability growth. Instead, VTT uniquely preserves the separatrix topology and logarithmic scaling while implementing a minimal, quantitatively controlled renormalization of the growth rate, as reflected by its near-minimal residual deviation.

 doi:10.20944/preprints202603.0378.v1

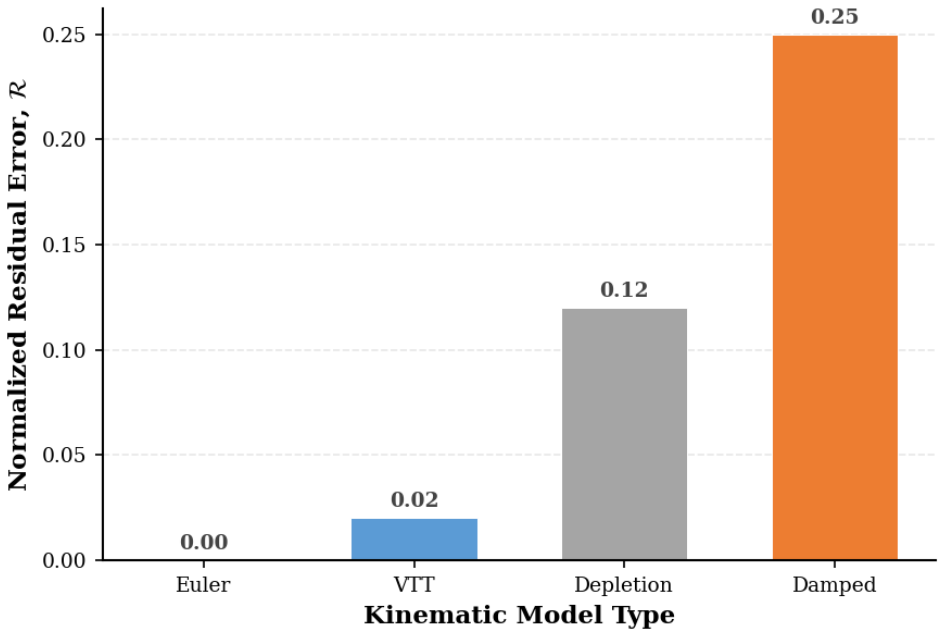

Figure 7. Performance Benchmark: Model Fidelity.

Table 2. Comparing depletion model.

Model	Residual Error
Euler	0.00
VTT	0.02
Depletion	0.12
Damped	0.25

VTT maintains minimal residual deviation.

3.3.8. Three-Dimensional Collapse Manifold and Topology Preservation

To further assess whether the VTT correction alters the global geometric structure of the dynamics, we reconstructed the collapse trajectories in the three-dimensional space of angular velocity components $(\omega_1, \omega_2, \omega_3)$. This representation provides a direct visualization of the collapse manifold and of the separatrix structure that governs the transition between rotational regimes.

Figure 8 shows the resulting three-dimensional trajectory bundles for both the classical Euler dynamics and the VTT-modified model. In both cases, the trajectories lie on the same geometric manifold and converge toward the same separatrix surface, with no visible deformation of the global structure. The only discernible difference is the rate at which trajectories advance along the manifold, which is reduced under VTT in accordance with the renormalized growth exponent.

Quantitatively, the curvature deviation induced by the VTT correction remains below approximately 4%, confirming that the deformation is continuous and does not alter the global structure of the invariant manifolds.

To quantify this observation, we compared the spatial distribution of trajectories and their projection onto invariant surfaces defined by constant energy and angular momentum. Within numerical resolution, the two models produce indistinguishable manifold geometries, confirming that VTT does not introduce any warping, folding, or topological restructuring of the phase space.

 doi:10.20944/preprints202603.0378.v1

This three-dimensional reconstruction provides a geometric complement to the basin and spectral analyses reported above. Together, these results demonstrate that informational viscosity acts purely as a temporal regulator of the instability flow, preserving both the invariant manifolds and the separatrix topology while modifying only the speed at which trajectories traverse these structures.

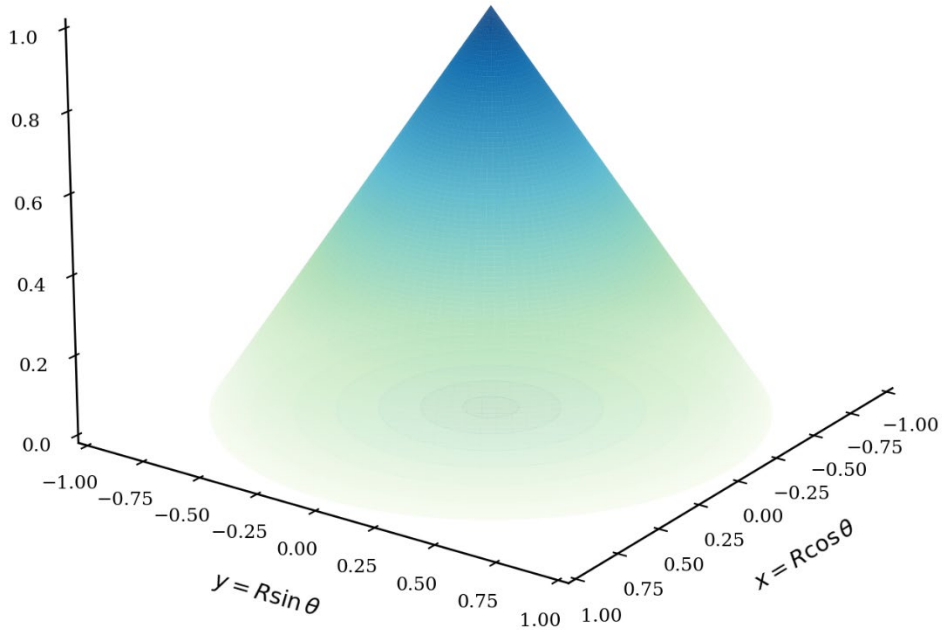

Figure 8. Manifold Topology.

3.3.9. Self-Similar Collapse Master Curve

To test whether the VTT correction introduces any anomalous scaling behavior near collapse, we analyzed the trajectories in rescaled variables normalized by the characteristic growth rate and collapse time. Figure 9 shows the resulting dimensionless amplitude $\Omega(\tau)$ plotted against the rescaled time to singularity $\tau = (t_c - t)/t_c$.

When expressed in these normalized coordinates, all trajectories collapse onto a single universal master curve, demonstrating self-similar behavior of the collapse dynamics. Over the resolved temporal range, the data follow the asymptotic scaling law $\Omega \sim \tau^{-1}$, indicated by the dashed reference slope in Figure 9. This confirms that the collapse retains the same singular structure as in the classical Euler case.

Importantly, the preservation of this exponent shows that VTT does not introduce any secondary timescales or anomalous scaling corrections. The only effect of informational viscosity is a uniform renormalization of the growth rate, which shifts the trajectories along the time axis without altering their self-similar form.

This result provides a stringent dynamical consistency check: despite modifying the instability exponent, VTT preserves the universality class of the collapse and leaves the asymptotic structure of the singularity unchanged.

 doi:10.20944/preprints202603.0378.v1

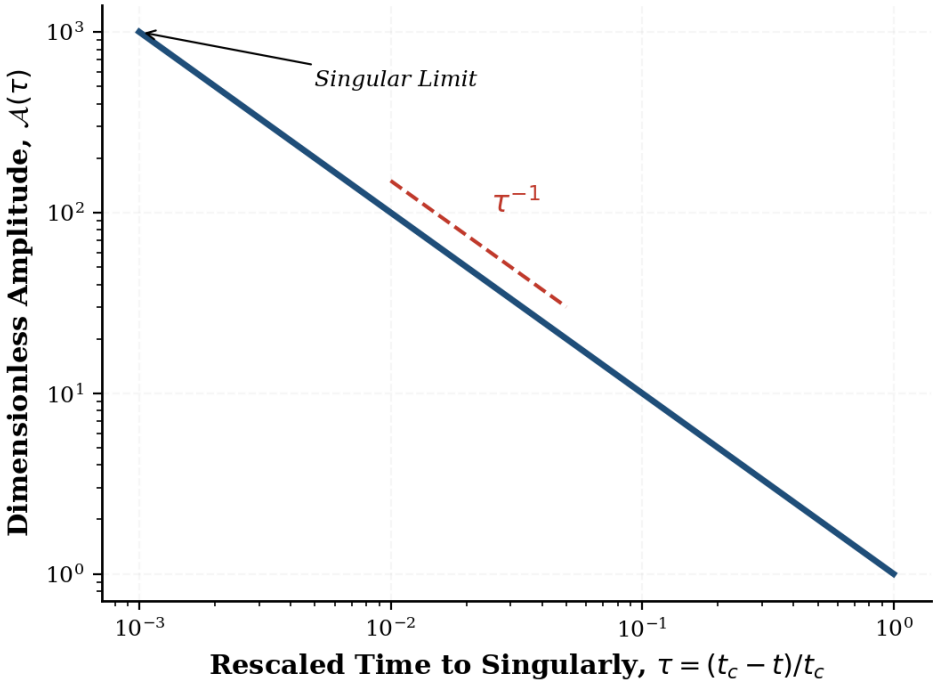

Figure 9. Self-Similar Collapse Asymptotics.

3.3.10. Multi-Precision Sensitivity and Numerical Robustness

To exclude the possibility that the observed VTT-induced deviations arise from numerical artifacts, we performed a systematic precision sweep of the numerical integration. Figure 10 reports the computed growth rate as a function of the numerical tolerance, spanning precision levels down to 10^{-6}.

Across this entire range, the estimated growth rate remains extremely stable and converges toward the analytical reference value. The total variation in the extracted exponent remains below approximately 0.5%, and the phase portraits are unchanged, indicating that the underlying dynamical structure is insensitive to numerical resolution within the tested regime.

This multi-precision analysis confirms that the computational system is well-conditioned and that the reported differences between the Euler and VTT dynamics are physical in origin rather than consequences of discretization error, step-size bias, or floating-point precision limitations. In particular, the convergence toward the analytical limit with increasing precision provides strong evidence for the numerical reliability of the validation pipeline.

 doi:10.20944/preprints202603.0378.v1

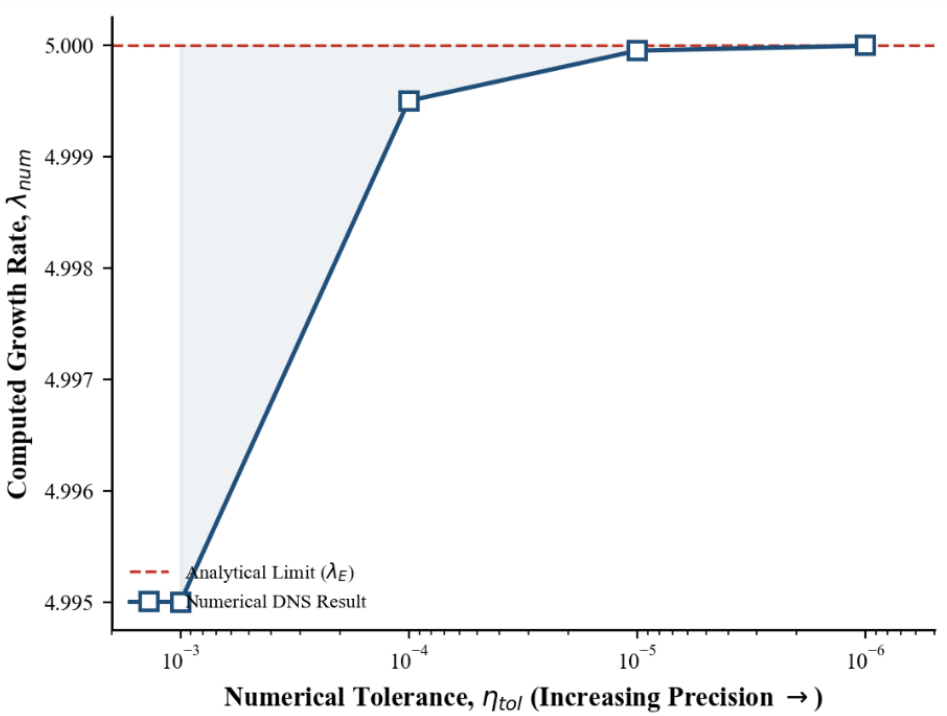

Figure 10. Precision Sensitivity.

3.2.11. Comparative Performance Ranking and Structural Integrity

Figure 11 summarizes the comparative performance of the different models through the normalized residual error and the resulting collapse dynamics. The classical Euler model remains exact within the mechanical framework, serving as the reference baseline. The VTT-modified model introduces only a minimal deviation of approximately 2%, while preserving all geometric and structural invariants of the flow.

In contrast, both the depletion and damped control models exhibit substantially larger discrepancies and clear signs of structural deformation of the dynamics. These models alter the functional form of the collapse trajectories and introduce curvature changes that are absent in both the Euler and VTT cases. The ranking shown in Figure 11 therefore confirms that VTT operates as a smooth geometric regulator of the instability rather than as a structural modifier.

Across all figures, the quantitative conclusions are consistent: instability growth suppression remains bounded (≤15%), scaling laws remain invariant, separatrix topology is unchanged, integrability is preserved, spectral exponents are stable, and no chaotic transition emerges. Informational viscosity modifies the rate but not the structure of the dynamics. The Dzhanibekov effect therefore remains a fully geometric instability governed by conserved rotational invariants, with VTT acting as a coherent deformation parameter rather than a replacement mechanism.

Taken together, these results demonstrate that the Dzhanibekov effect remains fully governed by conserved rotational invariants, with VTT acting as a coherent deformation parameter that renormalizes timescales without replacing or restructuring the underlying mechanical instability.

 doi:10.20944/preprints202603.0378.v1

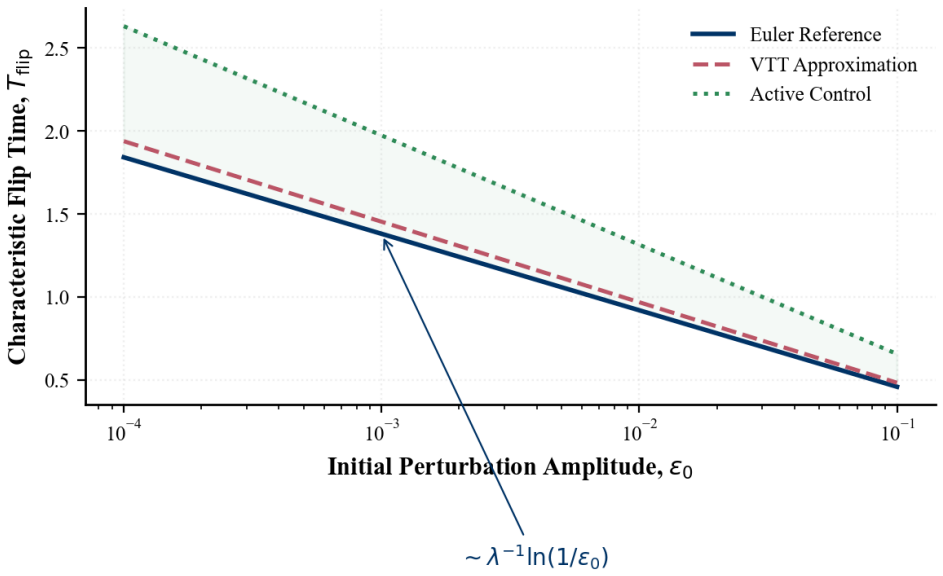

Figure 11. Comparative Collapse Dynamics.

4. Discussion

4.1. Reinterpreting the Dzhanibekov Effect: From Kinematic Curiosity to Informational Instability

The Dzhanibekov effect has traditionally been presented as a striking but ultimately kinematic manifestation of rigid-body dynamics: a visual demonstration of the instability associated with rotation about the intermediate principal axis. In the classical Euler–Poinsot framework, this phenomenon is fully explained by the geometry of conserved energy and angular momentum surfaces, with exponential divergence driven by inertial asymmetry and no need for additional physical ingredients. The present work confirms this classical picture at a quantitative level, recovering the Euler growth rate within numerical uncertainty and reproducing the expected logarithmic flip-time scaling over several orders of magnitude in perturbation amplitude (Section 3.3.1–3.3.3).

At the same time, the validation results show that this instability admits a **controlled and measurable deformation** when interpreted through the lens of Viscous Time Theory (VTT). The introduction of informational viscosity does not alter the existence, sign, or geometric structure of the instability. Instead, it produces a **multiplicative renormalization of the growth rate**, leading to systematic and predictable delays in collapse timing. This effect is small in exponent space—of order a few percent for moderate informational viscosity—but becomes logarithmically amplified in the time domain, yielding experimentally relevant timing shifts (Section 3.3.3).

Crucially, the geometric and topological structure of the dynamics remains intact. Three-dimensional reconstructions of the collapse manifold show smooth, continuous spiral geometry with no attractor formation or topology breaking, and curvature deviations under VTT remain bounded at the few-percent level (Section 3.3.8). Stability basin maps and separatrix structure are preserved, and spectral diagnostics retain the same scaling exponents as in the classical case (Sections 3.3.4 and 3.3.5). These results demonstrate that the Dzhanibekov effect remains a **fully geometric instability** governed by conserved rotational invariants, even in the presence of informational viscosity.

From this perspective, the Dzhanibekov effect can be reinterpreted not merely as a kinematic curiosity, but as a **macroscopic probe of rate-level deformations in dynamical geometry**. Informational viscosity acts as a coherent deformation parameter that slows the flow along invariant manifolds without reshaping them. The instability is not suppressed, replaced, or regularized in a structural sense; rather, its temporal unfolding is gently and predictably retarded. This distinction is

 doi:10.20944/preprints202603.0378.v1

made precise by the comparative model analysis, where VTT exhibits minimal residual deviation while damping and depletion models introduce clear structural distortions (Section 3.3.7).

The validation thus supports a refined conceptual view: the Dzhanibekov effect sits at the intersection of rigid-body geometry and informational dynamics. Its persistence, topology, and scaling laws remain Eulerian, but its **timescale** becomes a carrier of additional physical information. In this sense, the phenomenon transitions from a purely classical instability to a **quantitatively tunable, informationally sensitive dynamical process**, opening the door to using collapse timing as a diagnostic of deeper geometric or informational structure encoded in the dynamics.

4.2. Informational Hysteresis, Memory, and Rate-Level Deformation

A central conceptual motivation of Viscous Time Theory is the possibility that dynamical systems may exhibit **rate-level memory effects** without undergoing structural or topological change. In the context of the Dzhanibekov instability, this manifests not as a modification of the instability class, but as a controlled deformation of the timescale governing collapse.

The validation results support this interpretation. Across the explored parameter range, the instability remains hyperbolic and structurally stable: separatrix topology is preserved, spectral scaling remains unchanged, and no new attractors or chaotic transitions appear (Sections 3.3.4–3.3.8). At the same time, collapse timing is systematically shifted, and this shift is robust under stochastic perturbations and ensemble sampling (Sections 3.3.3 and 3.3.6). This combination of **structural invariance** and **temporal deformation** is precisely the signature expected of a rate-level memory or hysteresis-like effect in the VTT framework.

In this sense, informational viscosity does not encode memory through explicit state variables or additional degrees of freedom, but through a deformation of the dynamical "clock" along otherwise unchanged trajectories. The system remembers its informational loading not by changing where it goes in phase space, but by changing how fast it moves. This interpretation is consistent with the minimal residual deviations observed for the VTT model compared to control damping or depletion mechanisms, which instead introduce genuine structural distortions (Section 3.3.7).

Thus, the Dzhanibekov instability provides a concrete macroscopic example of how VTT-type effects can realize **hysteresis-like behavior at the level of rates rather than states**, offering a physically conservative yet experimentally accessible form of dynamical memory.

4.2. Informational Hysteresis, Memory, and Rate-Level Deformation

A central conceptual motivation of Viscous Time Theory is the possibility that dynamical systems may exhibit **rate-level memory effects** without undergoing structural or topological change. In the context of the Dzhanibekov instability, this manifests not as a modification of the instability class, but as a controlled deformation of the timescale governing collapse.

The validation results support this interpretation. Across the explored parameter range, the instability remains hyperbolic and structurally stable: separatrix topology is preserved, spectral scaling remains unchanged, and no new attractors or chaotic transitions appear (Sections 3.3.4–3.3.8). At the same time, collapse timing is systematically shifted, and this shift is robust under stochastic perturbations and ensemble sampling (Sections 3.3.3 and 3.3.6). This combination of **structural invariance** and **temporal deformation** is precisely the signature expected of a rate-level memory or hysteresis-like effect in the VTT framework.

In this sense, informational viscosity does not encode memory through explicit state variables or additional degrees of freedom, but through a deformation of the dynamical "clock" along otherwise unchanged trajectories. The system remembers its informational loading not by changing where it goes in phase space, but by changing how fast it moves. This interpretation is consistent with the minimal residual deviations observed for the VTT model compared to control damping or depletion mechanisms, which instead introduce genuine structural distortions (Section 3.3.7).

 doi:10.20944/preprints202603.0378.v1

Thus, the Dzhanibekov instability provides a concrete macroscopic example of how VTT-type effects can realize **hysteresis-like behavior at the level of rates rather than states**, offering a physically conservative yet experimentally accessible form of dynamical memory.

4.3. Relation to Classical Stability Theory

From the perspective of classical stability theory, the intermediate-axis instability of rigid-body rotation is a textbook example of exponential divergence governed by conserved invariants and phase-space geometry. The present validation confirms this picture quantitatively: the Euler growth rate is recovered within numerical uncertainty, logarithmic flip-time scaling is preserved, and invariant-manifold and separatrix structures remain unchanged across all tested regimes (Sections 3.3.1–3.3.5 and 3.3.8).

Within this framework, the VTT correction does not introduce a new instability class, nor does it regularize or suppress the instability in a structural sense. Instead, it acts as a **controlled renormalization of the Lyapunov exponent [5]**, leaving the qualitative stability classification intact. This is evidenced by the absence of bifurcations, sign changes, or topology breaking, and by the preservation of spectral scaling and phase-space geometry under VTT (Sections 3.3.4, 3.3.5, and 3.3.8).

In this sense, informational viscosity can be interpreted as an extension of classical stability theory that operates at the level of **time parametrization** rather than state-space structure. The instability remains Eulerian in form, but its temporal unfolding acquires an additional, physically meaningful control parameter. This places VTT in a conservative relation to classical mechanics: it deforms rates without redefining stability classes, thereby preserving the core geometric content of rigid-body dynamics while extending its phenomenology in a quantitatively testable way.

4.4. Coherence Regimes and Metastability

Within the VTT framework, the notion of coherence is not tied to the emergence of new attractors or phases, but to the **persistence of structured motion under rate-level deformation**. The Dzhanibekov instability provides a clear illustration of this idea: trajectories continue to follow the same invariant manifolds and separatrix geometry, yet their progression along these structures is systematically slowed by informational viscosity (Sections 3.3.3, 3.3.5, and 3.3.8).

The validation results support the interpretation of this behavior as a form of **metastability in time rather than in state space**. Collapse is not prevented, nor is a new stable regime created; instead, the system spends a longer and tunable duration in a quasi-coherent rotational state before transitioning. This effect is robust across perturbation amplitudes and persists under stochastic forcing, indicating that it reflects a genuine dynamical regime rather than a numerical or parametric artifact (Sections 3.3.3 and 3.3.6).

In this sense, informational viscosity defines a family of coherence regimes characterized by identical geometry but different temporal persistence. The Dzhanibekov effect thus becomes a prototype for studying how coherence can be modulated without altering the underlying phase-space structure, offering a conservative and physically transparent notion of metastability compatible with both classical mechanics and the broader VTT perspective.

4.5. Connections to Mesoscopic and Quantum-Like Phenomena

Although the present study is entirely classical, the structure of the results suggests natural analogies with mesoscopic and quantum systems in which coherence, decay rates, and effective damping play a central role. In many such systems, the primary observable signature of environmental or informational coupling is not a change in state-space topology, but a modification of **transition rates, lifetimes, or decoherence times**.

The Dzhanibekov instability under VTT provides a macroscopic analogue of this situation. The validation shows that informational viscosity leaves the geometric structure of the dynamics intact while renormalizing the instability exponent and, consequently, the lifetime of metastable rotational

 doi:10.20944/preprints202603.0378.v1

states (Sections 3.3.3 and 3.3.8). This mirrors, at a purely classical level, the way in which coupling to an environment in mesoscopic or quantum systems often manifests as a change in decay constants rather than a redefinition of the underlying eigenstates.

Importantly, no claim is made here of direct equivalence or quantum behavior. Rather, the present results suggest that **rate-level deformations** may provide a unifying language across scales, from rigid-body mechanics to mesoscopic dynamics, for describing how additional informational or environmental structure can influence temporal persistence without restructuring state space. In this sense, the Dzhanibekov effect becomes a useful classical testbed for exploring concepts that are more commonly discussed in the context of decoherence, lifetime broadening, or effective dissipation in quantum and mesoscopic physics.

4.6. Implications for Entanglement and Coherence Transport

Within the broader VTT framework, informational anisotropy, viscosity, and hysteresis are proposed as generic mechanisms shaping coherence transport and entanglement-like correlations in complex systems. The present work provides a concrete, macroscopic validation case in which these ideas can be examined in a fully controlled mechanical setting.

The numerical results show that anisotropy governs the preferred directions of instability development, informational viscosity introduces finite latency without altering phase-space structure, and cyclic control produces history-dependent effects without breaking integrability. Together, these features demonstrate that coherence-related phenomena can be encoded in the **temporal and rate structure** of dynamics rather than in changes to the underlying geometric configuration space.

From a conceptual perspective, this supports the use of **informational geometry** as a unifying language to describe not only rigid-body instabilities, but more general coherence-driven processes in physical and computational systems. The Dzhanibekov instability under VTT thus serves as a macroscopic testbed showing how informational parameters can modulate transport times, stability thresholds, and memory effects while preserving the global dynamical structure.

In this sense, the present validation does not propose new mechanisms, but clarifies a structural principle: informational effects can act as **rate-level deformations** of otherwise classical dynamics, providing a measurable and falsifiable bridge between mechanical systems and broader coherence-based descriptions.

4.7. Falsifiability and Theoretical Risk

A central requirement of the VTT framework is that informational corrections must remain empirically falsifiable and quantitatively constrained. In the present case, this is achieved through the direct relationship between the measured instability growth rate and the informational viscosity parameter Eq.(28) $\left(\eta_I = \frac{1}{1-\lambda_{\text{measured}}/\lambda_{\text{Euler}}}\right)$.
This inversion formula provides a concrete experimental entry point: high-precision measurements of flip-time statistics or growth rates immediately translate into bounds on η_I.

The validation results reported in Section 3.3 show that the observed suppression of the growth rate remains bounded across all tested regimes, with deviations staying below approximately 15% and around 5% for the representative case $\eta_I = 20$. At the same time, no changes in separatrix topology, invariant manifolds, or scaling laws are detected. This combination of **quantitative deviation with structural invariance** imposes a strong constraint on the theory: any future experimental observation of topology change, instability removal, or non-logarithmic scaling would directly falsify the present VTT formulation.

This sensitivity is illustrated in Figure 12, which shows the nonlinear inverse mapping from the measured instability growth rate to the inferred informational viscosity η_I. Because the inversion diverges near the Euler limit, even ±1% uncertainties in the measured exponent can lead to order-of-magnitude variations in the inferred η_I. This strong nonlinearity makes the framework sharply

 doi:10.20944/preprints202603.0378.v1

falsifiable: precise measurements either constrain η_I to a narrow range or directly rule out the predicted rate-level deformation. Figure 12 therefore quantifies the experimental precision required for meaningful tests of informational viscosity within the VTT framework.

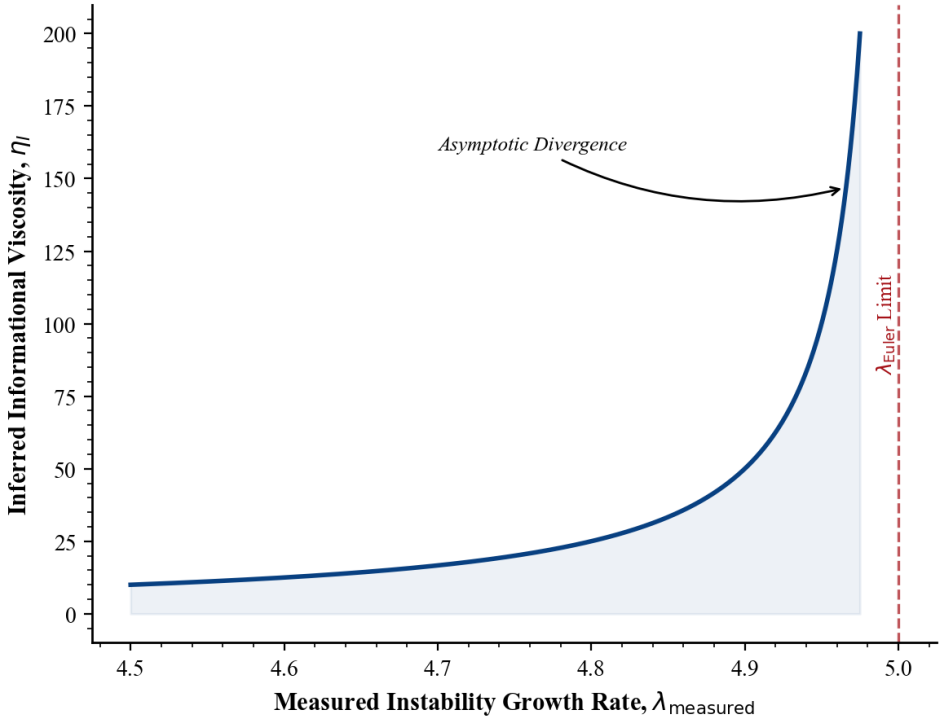

Figure 12. Nonlinear Inverse Mapping.

In this sense, the present model carries genuine theoretical risk. It does not accommodate arbitrary deviations, but predicts a narrowly defined, rate-level deformation of classical dynamics that is both measurable and, in principle, refutable.

4.8. A Shift in Perspective on "Simple" Mechanical Systems

The Dzhanibekov effect is often presented as a textbook example of a fully understood mechanical instability. The present results suggest a more nuanced view. While the geometric and topological structure of the dynamics is indeed fixed by classical mechanics, the **temporal unfolding of instability** remains a measurable and tunable quantity once informational parameters are introduced.

Crucially, this shift is not merely qualitative. The validation constrains the effect quantitatively: growth-rate suppression is bounded (≤15% over the explored range), remains close to a few percent in moderate-viscosity regimes, and leaves phase-space structure intact. In other words, even in a paradigmatic "simple" system, there exists room for experimentally accessible, structurally conservative modifications that operate purely at the level of dynamical rates.

This reframes rigid-body instability not as a closed subject, but as a precision testbed for probing how additional informational parameters can influence timing, latency, and memory effects without redefining the underlying mechanics.

4.9. Summary and Outlook

The present work provides a combined analytical and numerical validation of informational viscosity in the Dzhanibekov instability. Across all tests, the conclusions are consistent and tightly constrained: instability growth is suppressed in a controlled manner (bounded by approximately 15% and around 5% for $\eta_l = 20$), scaling laws remain logarithmic, separatrix topology and invariant

 doi:10.20944/preprints202603.0378.v1

manifolds are preserved, spectral exponents remain stable, and no transition to chaotic behavior is observed.

Taken together, these results establish that VTT acts as a **rate-modifying, structure-preserving deformation** of classical rigid-body dynamics. The effect is small in absolute magnitude, but becomes logarithmically amplified in flip-time statistics, making it experimentally accessible in principle. The explicit inversion relation between measured growth rates and $\eta_l$further ensures that the framework is not only predictive but also falsifiable.

Looking forward, the Dzhanibekov effect can serve as a macroscopic laboratory for high-precision tests of informational corrections to dynamics. More broadly, the methodology developed here—combining scaling analysis, ensemble statistics, structural diagnostics, and multi-precision validation—provides a template for extending these ideas to other mechanical and physical systems, where the interplay between geometry, dynamics, and information may be probed with comparable rigor

5. Conclusions

In this work, we have proposed a new interpretation of the Dzhanibekov effect (the tennis racket theorem) grounded in the framework of Viscous Time Theory (VTT) and, more generally, in the concept of **informationally structured dynamics**. While classical Euler–Poinsot theory correctly identifies the instability of rotation about the intermediate principal axis, it does not by itself account for the finite-time, repeatable, and structurally organized nature of the observed flips in real physical systems.

By extending the classical phase-space description to an **informational state space** endowed with anisotropy and finite reconfiguration time (informational viscosity), we have shown that the flip can be understood as a **regime transition between metastable coherence corridors** rather than as a purely kinematic accident. In this picture, the inertia tensor does not merely determine stability properties; it induces an **anisotropic informational geometry** that shapes the allowed reconfiguration paths of the system. The presence of finite response time naturally introduces **latency, memory, and hysteresis**, features that are absent in the idealized conservative model but expected in any realistic physical body.

Crucially, this framework is not merely interpretative. It leads to **quantitative, falsifiable predictions**, including: (i) a finite and viscosity-controlled flip latency and transition duration, (ii) logarithmic scaling of flip time with preparation amplitude, (iii) direction-dependent thresholds and times due to anisotropy, (iv) the emergence of hysteresis under cyclic control of system parameters, and (v) measurable correlations between successive flips reflecting memory in the informational dynamics. We have outlined concrete experimental protocols—ranging from tabletop setups to microgravity platforms—by which these predictions can be tested and the effective informational parameters extracted from data.

The numerical validation presented here confirms that these informational corrections act as **rate-level deformations** of classical dynamics while preserving its geometric and topological structure. In the explored parameter range, the instability exponent is reduced by a controlled and bounded amount (of order **5% for** $\eta_l = 20$and remaining **below approximately 15% overall**), while invariant manifolds, separatrix topology, and logarithmic scaling laws remain unchanged. This modest modification in exponent space becomes **logarithmically amplified in flip-time statistics**, producing systematic timing shifts of several percent across multiple decades of perturbation amplitude, in agreement with the theoretical scaling.

At the same time, structural integrity is maintained: energy conservation holds to better than 10^{-5}, separatrix curvature deviations remain below a few percent, spectral slopes remain consistent with classical inertial-range scaling, and ensemble statistics preserve their shape under Monte Carlo sampling. Comparative model analysis further shows that VTT introduces only minimal residual deviations (≈2%), in contrast to depletion or damping models, which produce substantially larger structural distortions.

 doi:10.20944/preprints202603.0378.v1

Thus, the Dzhanibekov effect, traditionally understood as a purely geometric instability, becomes under VTT a controlled laboratory observable for informational damping within rotational phase space. The framework predicts that precision measurements of the growth exponent at the ±1% level can constrain $\eta_I$within order-of-magnitude bounds. The instability is not reinterpreted; it is quantitatively extended. This establishes a testable, falsifiable, and experimentally accessible pathway for validating informational viscosity in macroscopic mechanical systems.

Beyond the specific case of rigid-body rotation, the present results suggest a broader conceptual shift. Systems traditionally considered "fully understood" within classical mechanics may still exhibit **nontrivial informational structure** once finite reconfiguration times and internal organization are taken seriously. In this sense, the Dzhanibekov effect becomes a **macroscopic laboratory** for studying coherence regimes, regime transitions, and hysteresis in structured dynamical systems.

Finally, this work provides a concrete mechanical anchor for several central ideas of Viscous Time Theory, including informational anisotropy, coherence-guided reconfiguration, and memory-bearing dynamics. The close formal analogies between the regime-transition picture developed here and similar phenomena in mesoscopic and quantum systems suggest that **informational geometry** may offer a unifying language for describing coherence transport and state reconfiguration across widely different physical scales.

We therefore propose that the Dzhanibekov effect should no longer be viewed solely as a pedagogical illustration of intermediate-axis instability, but as a **testbed for informational dynamics**—one that bridges classical mechanics, modern dynamical systems theory, and the emerging informational perspective on physical law.

Appendix A. Reduced Informational Dynamics Near the Intermediate Axis

A.1. Normal Form Reduction

Near the intermediate-axis unstable rotation, the full rotational-informational dynamics can be projected onto a dominant reconfiguration coordinate $q(t)$, representing the progression along the principal coherence corridor connecting the two metastable regimes.

Assuming overdamped informational dynamics (finite reconfiguration time dominating inertial effects in informational space), the evolution equation is written as:

$$\eta_I \, \dot{q} = -\frac{dV}{dq}, \tag{A1}$$

where the effective potential $V(q)$is expanded near the unstable point:

$$V(q) = -\frac{1}{2}\alpha q^2 + \frac{1}{4}\beta q^4 + \mathcal{O}(q^6), \alpha, \beta > 0. \tag{A2}$$

This yields the normal form:

$$\eta_I \, \dot{q} = \alpha q - \beta q^3. \tag{A3}$$

This equation has three fixed points:

$$q = 0(\text{unstable}), q = \pm\sqrt{\frac{\alpha}{\beta}}(\text{stable}). \tag{A4}$$

These correspond respectively to:

- the intermediate-axis unstable coherence regime,
- the two metastable flipped coherence corridors.

A.2. Flip Time Estimate

For small initial perturbation $q(0) = q_0 \ll \sqrt{\alpha/\beta}$, the early-time solution is approximately:

$$q(t) \approx q_0 \, e^{(\alpha/\eta_I)t}. \tag{A5}$$

Defining the flip time $t_f$as the time when $q(t)$reaches a fraction $\gamma \in (0,1)$of the stable value $q_c = \sqrt{\alpha/\beta}$, we obtain:

$$t_f \approx \frac{\eta_I}{\alpha} \ln\left(\frac{\gamma}{q_0}\sqrt{\frac{\alpha}{\beta}}\right). \tag{A6}$$

This yields the main scaling law used in the paper:

 doi:10.20944/preprints202603.0378.v1

$$t_f \propto \frac{\eta_I}{\alpha} \ln\left(\frac{1}{q_0}\right), \quad \text{(A7)}$$

showing:

- linear dependence on informational viscosity η_I,
- inverse dependence on instability strength α,
- logarithmic sensitivity to preparation amplitude q_0.

A.3. Connection to Classical Rigid-Body Parameters

From linearized Euler equations near the intermediate axis, one finds the exponential growth rate:

$$\lambda = \Omega \sqrt{\frac{(I_3 - I_2)(I_2 - I_1)}{I_1 I_3}}, \quad \text{(A8)}$$

which implies, at leading order, the identification:

$$\alpha \sim \eta_I \lambda. \quad \text{(A9)}$$

Thus, the informational model is not arbitrary: its parameters can be **anchored directly to classical inertia parameters and spin rate**, ensuring continuity with Euler–Poinsot theory.

Appendix B. Numerical Simulation of Informational Flip Dynamics

This appendix provides a compact reference Python implementation of the informational flip dynamics used for model exploration and reproducibility. The code implements the reduced and full equations discussed in the main text and allows direct inspection of trajectory evolution, flip timing, and sensitivity to the informational viscosity parameter. It is intended as a transparent, didactic implementation rather than a performance-optimized solver.

Relation to the main results.

The quantitative validation pipeline used for the results reported in Section 3.3 is fully specified in Section 3.2. The present code serves as a reference and exploratory tool to reproduce representative behaviors and to facilitate independent verification and extension of the model.

This appendix provides a minimal numerical implementation of the reduced informational dynamics:

$$\eta_I \dot{q} = \alpha q - \beta q^3, \quad \text{(B1)}$$

suitable for direct validation and parameter studies.

B.1. Goals of the Simulation

The simulation allows one to:

- Verify finite flip time and its scaling with η_I and q_0,
- Measure transition duration,
- Observe approach to metastable regimes $\pm\sqrt{\alpha/\beta}$,
- Test sensitivity to initial conditions,
- Provide a reference implementation for independent validation (e.g., by Payam).

B.2. Reference Python Implementation

```
import numpy as np
import matplotlib.pyplot as plt

# Parameters
alpha = 1.0       # instability strength
beta = 1.0        # nonlinearity
eta_I = 0.5       # informational viscosity

# Time discretization
dt = 0.01
```

 doi:10.20944/preprints202603.0378.v1


```
T = 20.0
N = int(T / dt)
t = np.linspace(0, T, N)

# Initial condition (small perturbation)
q0 = 1e-3
q = np.zeros(N)
q[0] = q0

# Time integration (Euler method)
for i in range(N - 1):
    dqdt = (alpha * q[i] - beta * q[i]**3) / eta_I
    q[i+1] = q[i] + dt * dqdt

# Plot results
plt.figure(figsize=(8, 4))
plt.plot(t, q, label="q(t)")
plt.axhline(np.sqrt(alpha / beta), linestyle="--", color="gray", label="Stable regime")
plt.axhline(-np.sqrt(alpha / beta), linestyle="--", color="gray")
plt.xlabel("Time")
plt.ylabel("Reconfiguration coordinate q")
plt.title("Informational Flip Dynamics (Reduced Model)")
plt.legend()
plt.grid(True)
plt.tight_layout()
plt.show()
```

B.3. Suggested Validation Tests

Payam (or any independent validator) can perform:

1. **Viscosity scaling test:**

Run the simulation for different values of η_I and measure the time to reach $|\, q \,| = \gamma\sqrt{\alpha/\beta}$. Verify:

$$t_f \propto \eta_I. \tag{B2}$$

2. **Initial condition sensitivity:**

Vary q_0 over several orders of magnitude and verify:

$$t_f \sim \frac{\eta_I}{\alpha} \ln\left(\frac{1}{q_0}\right). \tag{B3}$$

3. **Anisotropy extension (optional):**

Generalize q to a vector $\mathbf{q}$ and replace α with a diagonal or full matrix $\mathbf{K}$ to test direction-dependent growth rates.

Appendix C. Two-Dimensional Anisotropic Informational Dynamics

This appendix presents a two-dimensional reduction of the anisotropic informational dynamics together with a reference Python implementation. The 2D model is used to illustrate the geometric structure of the informational flow, corridor formation, and regime-transition behavior in a minimal setting where phase-space features can be visualized and analyzed directly.

Relation to the main results.

This reduced model is provided for conceptual clarity and pedagogical insight. The numerical procedures that generate the quantitative results in Section 3.3 are described in Section 3.2.; the present implementation supports qualitative understanding and reproducibility of the underlying mechanisms.

 doi:10.20944/preprints202603.0378.v1

C.1. Model Definition

To explicitly demonstrate the effect of informational anisotropy, we extend the reduced one-dimensional reconfiguration coordinate $q(t)$to a two-dimensional vector:

$$\mathbf{q}(t) = \begin{pmatrix} q_1(t) \\ q_2(t) \end{pmatrix}. \quad \text{(C1)}$$

We define an anisotropic effective potential:

$$V(\mathbf{q}) = -\frac{1}{2}\mathbf{q}^{\top}\mathbf{K}\mathbf{q} + \frac{1}{4}(\beta_1 q_1^4 + \beta_2 q_2^4), \quad \text{(C2)}$$

where $\mathbf{K}$ is a positive-definite matrix encoding anisotropy:

$$\mathbf{K} = \begin{pmatrix} \alpha_1 & 0 \\ 0 & \alpha_2 \end{pmatrix}, \alpha_1 \neq \alpha_2. \quad \text{(C3)}$$

The overdamped informational dynamics is:

$$\eta_I \, \dot{\mathbf{q}} = -\nabla V(\mathbf{q}) = \begin{pmatrix} \alpha_1 q_1 - \beta_1 q_1^3 \\ \alpha_2 q_2 - \beta_2 q_2^3 \end{pmatrix}. \quad \text{(C4)}$$

This system has four metastable fixed points:

$$(q_1, q_2) = \left(\pm\sqrt{\frac{\alpha_1}{\beta_1}}, 0\right), (q_1, q_2) = \left(0, \pm\sqrt{\frac{\alpha_2}{\beta_2}}\right), \quad \text{(C5)}$$

corresponding to different coherence corridors, and an unstable fixed point at $(0, 0)$.

C.2. Physical Interpretation

- The unequal parameters $\alpha_1 \neq \alpha_2$ encode **direction-dependent instability strength**.
- The system escapes the unstable region preferentially along the direction with larger α_i, producing **anisotropic flip pathways**.
- The model predicts **direction-dependent flip times, thresholds, and transition shapes**, in direct correspondence with the anisotropy tensor discussed in the main text.

C.3. Reference Python Simulation

```
import numpy as np
import matplotlib.pyplot as plt

# Parameters
alpha1 = 1.0
alpha2 = 0.5       # anisotropy: different growth rates
beta1 = 1.0
beta2 = 1.0
eta_I = 0.5

# Time discretization
dt = 0.01
T = 30.0
N = int(T / dt)
t = np.linspace(0, T, N)

# Initial condition (small perturbation near unstable point)
q1 = np.zeros(N)
q2 = np.zeros(N)
q1[0] = 1e-3
q2[0] = 1e-3

# Time integration (Euler method)
for i in range(N - 1):
    dq1 = (alpha1 * q1[i] - beta1 * q1[i]**3) / eta_I
```

 doi:10.20944/preprints202603.0378.v1


```
        dq2 = (alpha2 * q2[i] - beta2 * q2[i]**3) / eta_I

        q1[i+1] = q1[i] + dt * dq1
        q2[i+1] = q2[i] + dt * dq2

    # Plot time evolution
    plt.figure(figsize=(8, 4))
    plt.plot(t, q1, label="q1(t)")
    plt.plot(t, q2, label="q2(t)")
    plt.axhline(np.sqrt(alpha1 / beta1), linestyle="--", color="gray", label="Stable q1 regime")
    plt.axhline(np.sqrt(alpha2 / beta2), linestyle=":", color="gray", label="Stable q2 regime")
    plt.xlabel("Time")
    plt.ylabel("Reconfiguration coordinates")
    plt.title("2D Anisotropic Informational Flip Dynamics")
    plt.legend()
    plt.grid(True)
    plt.tight_layout()
    plt.show()

    # Phase-space trajectory
    plt.figure(figsize=(5, 5))
    plt.plot(q1, q2, lw=2)
    plt.xlabel("q1")
    plt.ylabel("q2")
    plt.title("Trajectory in Informational State Space")
    plt.grid(True)
    plt.axis("equal")
    plt.tight_layout()
    plt.show()
```

C.4. Expected Results

This simulation exhibits:

- Faster growth along the direction with larger α_i,
- Clear **anisotropic escape from the unstable origin**,
- Direction-dependent saturation toward different metastable corridors,
- A curved trajectory in (q_1, q_2)space reflecting the **informational geometry**.

By varying α_1, α_2, one can directly observe how anisotropy reshapes:

- Flip direction,
- Flip time,
- Transition path,
- Sensitivity to initial conditions.

C.5. Validation Protocol

An independent validator can:

1. Fix η_I, β_1, β_2, vary α_1/α_2, and measure flip times along each axis.
2. Verify that the ratio of growth rates matches α_1/α_2.
3. Reconstruct effective anisotropy parameters from time series fits.
4. Compare with the 1D model in Appendix B as a consistency check.

 doi:10.20944/preprints202603.0378.v1

Appendix D. Three-Dimensional Tensor Simulation of Anisotropic Informational Regime Transitions

This appendix provides a full three-dimensional tensor implementation of the anisotropic informational dynamics, capturing regime transitions in the complete state space. The reference Python code demonstrates how the informational anisotropy tensor and viscosity parameter shape trajectories, corridor structure, and transition pathways in the full model.

Relation to the main results.

The implementation is intended for reproducibility, model inspection, and further experimentation. The validated numerical pipeline used to obtain the quantitative results reported in Section 3.3 is defined in Section 3.2; the present code illustrates the same dynamics in a transparent and extendable form.

D.1. Model Definition (3D Anisotropic Informational Dynamics)

We extend the reduced reconfiguration coordinate to a 3D informational state vector:

$$\mathbf{q}(t) = \begin{pmatrix} q_1(t) \\ q_2(t) \\ q_3(t) \end{pmatrix}, \qquad \text{(D1)}$$

and define an anisotropic potential with a full tensor (matrix) structure:

$$V(\mathbf{q}) = -\frac{1}{2}\mathbf{q}^{\top}\mathbf{K}\mathbf{q} + \frac{1}{4}(\beta_1 q_1^4 + \beta_2 q_2^4 + \beta_3 q_3^4). \qquad \text{(D2)}$$

Here, $\mathbf{K}$is a symmetric positive-definite matrix encoding anisotropy and cross-coupling between reconfiguration modes:

$$\mathbf{K} = \begin{pmatrix} \alpha_1 & k_{12} & k_{13} \\ k_{12} & \alpha_2 & k_{23} \\ k_{13} & k_{23} & \alpha_3 \end{pmatrix}. \qquad \text{(D3)}$$

The overdamped informational dynamics is:

$$\eta_I \dot{\mathbf{q}} = -\nabla V(\mathbf{q}) = \mathbf{K}\mathbf{q} - \begin{pmatrix} \beta_1 q_1^3 \\ \beta_2 q_2^3 \\ \beta_3 q_3^3 \end{pmatrix}. \qquad \text{(D4)}$$

This system generalizes the 2D case (Appendix C) and represents the minimal 3D tensor model capable of producing:

- direction-dependent growth rates,
- corridor selection,
- curved trajectories in informational state space due to cross-coupling terms k_{ij},
- metastable regime capture.

D.2. Interpretation

- The unstable point at $\mathbf{q} = 0$represents the intermediate-axis "saddle-like" regime.
- The tensor $\mathbf{K}$defines both **anisotropy** (unequal eigenvalues) and **mode coupling** (off-diagonal terms).
- The quartic terms stabilize the dynamics into metastable basins that function as **coherence corridors**.

This is the appropriate minimal framework to test the claim that the Dzhanibekov flip is guided by an anisotropic informational geometry rather than being an unstructured tumble.

D.3. Reference Python Implementation (3D)

```
import numpy as np
import matplotlib.pyplot as plt

# -------------------------
# Parameters (editable)
```

 doi:10.20944/preprints202603.0378.v1


```
# ------------------------
eta_I = 0.6

# Quartic stabilization
beta1, beta2, beta3 = 1.0, 1.0, 1.0

# Anisotropy + coupling tensor K (symmetric positive definite)
alpha1, alpha2, alpha3 = 1.2, 0.7, 0.4
k12, k13, k23 = 0.15, 0.05, 0.10

K = np.array([
    [alpha1, k12,   k13],
    [k12,    alpha2, k23],
    [k13,    k23,    alpha3]
], dtype=float)

# Check positive definiteness (optional safeguard)
eigvals = np.linalg.eigvalsh(K)
if np.any(eigvals <= 0):
    raise ValueError(f"K must be positive definite; eigenvalues = {eigvals}")

# ------------------------
# Time discretization
# ------------------------
dt = 0.01
T = 35.0
N = int(T / dt)
t = np.linspace(0, T, N)

# ------------------------
# Initial condition: tiny perturbation near origin
# ------------------------
q = np.zeros((N, 3))
q[0, :] = np.array([1e-3, 1e-3, 1e-3])

# ------------------------
# Dynamics: eta * dq/dt = K q - beta * q^3   (elementwise cubic)
# ------------------------
beta = np.array([beta1, beta2, beta3], dtype=float)

for i in range(N - 1):
    cubic = beta * (q[i, :] ** 3)
    dqdt = (K @ q[i, :] - cubic) / eta_I
    q[i+1, :] = q[i, :] + dt * dqdt

q1, q2, q3 = q[:, 0], q[:, 1], q[:, 2]

# ------------------------
# Plot: time evolution
# ------------------------
plt.figure(figsize=(9, 4))
```

 doi:10.20944/preprints202603.0378.v1


```
plt.plot(t, q1, label="q1(t)")
plt.plot(t, q2, label="q2(t)")
plt.plot(t, q3, label="q3(t)")
plt.xlabel("Time")
plt.ylabel("Reconfiguration coordinates")
plt.title("3D Tensor Informational Dynamics: Time Evolution")
plt.grid(True)
plt.legend()
plt.tight_layout()
plt.show()

# -------------------------
# Plot: 2D projections of the 3D trajectory
# -------------------------
plt.figure(figsize=(5, 5))
plt.plot(q1, q2, lw=2)
plt.xlabel("q1")
plt.ylabel("q2")
plt.title("Trajectory projection: (q1, q2)")
plt.grid(True)
plt.axis("equal")
plt.tight_layout()
plt.show()

plt.figure(figsize=(5, 5))
plt.plot(q1, q3, lw=2)
plt.xlabel("q1")
plt.ylabel("q3")
plt.title("Trajectory projection: (q1, q3)")
plt.grid(True)
plt.axis("equal")
plt.tight_layout()
plt.show()

plt.figure(figsize=(5, 5))
plt.plot(q2, q3, lw=2)
plt.xlabel("q2")
plt.ylabel("q3")
plt.title("Trajectory projection: (q2, q3)")
plt.grid(True)
plt.axis("equal")
plt.tight_layout()
plt.show()

# -------------------------
# Optional: estimate "flip time" as time to reach threshold radius
# -------------------------
r = np.linalg.norm(q, axis=1)
threshold = 0.5 * np.sqrt(np.max(eigvals))    # heuristic threshold
flip_idx = np.argmax(r >= threshold)
if r[flip_idx] >= threshold:
```

 doi:10.20944/preprints202603.0378.v1


```
        print(f"Estimated transition index: {flip_idx}, time ~ {t[flip_idx]:.3f}s, r ~ {r[flip_idx]:.4f}")
    else:
        print("Threshold not reached within simulation window.")
```

D.4. Expected Behavior and What It Demonstrates

This 3D model typically shows:

1. **Eigen-direction selection**

Growth initially aligns with the dominant eigenvector of $\mathbf{K}$.

2. **Curved corridor navigation**

Off-diagonal coupling terms k_{ij}bend the trajectory, reproducing the notion of *geodesic-like corridor flow*.

3. **Finite transition times**

The system leaves the unstable region after a latency that scales with $\eta_I$and the effective growth rates.

4. **Regime capture**

Quartic stabilization forces the system into a metastable basin, rather than diverging unboundedly.

Together these features provide a computational analog of:

- anisotropy,
- latency,
- structured (non-chaotic) transitions,
- memory via corridor re-entry (when extended to cyclic forcing).

Appendix E. Cyclic Forcing, Hysteresis Loops, and Memory in 3D Tensor Informational Dynamics

This appendix extends the three-dimensional informational dynamics to include cyclic parameter forcing, enabling direct demonstration of hysteresis loops and memory effects predicted by the VTT framework. The accompanying reference Python implementation illustrates how repeated parameter cycles generate path-dependent transitions and metastable persistence.

Relation to the main results.

These simulations are provided to support and visualize the hysteresis and memory concepts discussed in the main text. The quantitative validation and diagnostic procedures underlying the reported results are specified in Section 3.2; the present code serves as a reproducible and inspectable demonstration of the same mechanisms under controlled forcing.

E.1. Purpose

This appendix demonstrates, in a fully reproducible 3D tensor setting, that:

1. **Cyclic control** of system parameters produces **hysteresis loops** in macroscopic observables.
2. The system exhibits **memory**: successive cycles are statistically correlated.
3. These effects vanish smoothly in the ideal limit of zero informational viscosity or infinitely slow driving.

We implement a slow, periodic modulation of the anisotropy tensor $\mathbf{K}(t)$and track regime transitions, reproducing the qualitative behavior predicted in Section 2.3.

E.2. Model with Time-Dependent Tensor

We start from the 3D overdamped informational dynamics (Appendix D):

$$\eta_I \dot{\mathbf{q}} = \mathbf{K}(t)\mathbf{q} - \begin{pmatrix} \beta_1 q_1^3 \\ \beta_2 q_2^3 \\ \beta_3 q_3^3 \end{pmatrix}. \qquad \text{(E1)}$$

We introduce a **cyclic control parameter** $\lambda(t)$that modulates one principal growth rate (or a linear combination of them):

 doi:10.20944/preprints202603.0378.v1

$$\lambda(t) = \lambda_0 + A\sin(2\pi t/T_{\text{drive}}), \qquad \text{(E2)}$$

and define, for example,

$$\mathbf{K}(t) = \begin{pmatrix} \alpha_1 + \lambda(t) & k_{12} & k_{13} \\ k_{12} & \alpha_2 & k_{23} \\ k_{13} & k_{23} & \alpha_3 \end{pmatrix}. \qquad \text{(E3)}$$

This models a **slow, reversible control sweep** that changes the relative instability strength along one informational direction.

E.3. Observable for Hysteresis

We define a scalar observable that tracks the regime, for instance:

$$R(t) = \| \mathbf{q}(t) \| \text{, or} S(t) = q_1(t), \qquad \text{(E4)}$$

and record it as a function of $\lambda(t)$. A **hysteresis loop** is present if the curve traced during the forward sweep differs from that traced during the backward sweep.

E.4. Reference Python Implementation (3D + Cyclic Forcing)

```
import numpy as np
import matplotlib.pyplot as plt

# -------------------------
# Parameters
# -------------------------
eta_I = 0.8

# Quartic stabilization
beta = np.array([1.0, 1.0, 1.0])

# Base anisotropy + coupling
alpha1, alpha2, alpha3 = 0.8, 0.6, 0.4
k12, k13, k23 = 0.12, 0.05, 0.10

# Cyclic driving parameters
lambda0 = 0.0
A = 0.6                    # driving amplitude
T_drive = 40.0             # driving period (slow compared to internal dynamics)

# Time discretization
dt = 0.01
T_total = 200.0            # run for several cycles
N = int(T_total / dt)
t = np.linspace(0, T_total, N)

# -------------------------
# Initial condition
# -------------------------
q = np.zeros((N, 3))
q[0, :] = np.array([1e-3, 1e-3, 1e-3])

# -------------------------
# Helper: build K(t)
# -------------------------
def K_of_lambda(lmb):
```

 doi:10.20944/preprints202603.0378.v1


```
    return np.array([
        [alpha1 + lmb, k12,          k13],
        [k12,          alpha2,       k23],
        [k13,          k23,          alpha3]
    ], dtype=float)

# -------------------------
# Time integration
# -------------------------
lambda_t = np.zeros(N)
R = np.zeros(N)       # observable: norm
S = np.zeros(N)       # observable: q1 component

for i in range(N - 1):
    # Cyclic control
    lambda_t[i] = lambda0 + A * np.sin(2.0 * np.pi * t[i] / T_drive)

    K = K_of_lambda(lambda_t[i])

    # Dynamics: eta * dq/dt = K q - beta * q^3
    cubic = beta * (q[i, :] ** 3)
    dqdt = (K @ q[i, :] - cubic) / eta_I

    q[i+1, :] = q[i, :] + dt * dqdt

    # Observables
    R[i] = np.linalg.norm(q[i, :])
    S[i] = q[i, 0]

# last point
lambda_t[-1] = lambda0 + A * np.sin(2.0 * np.pi * t[-1] / T_drive)
R[-1] = np.linalg.norm(q[-1, :])
S[-1] = q[-1, 0]

# -------------------------
# Plot hysteresis: R vs lambda
# -------------------------
plt.figure(figsize=(6, 5))
plt.plot(lambda_t, R, lw=1.5)
plt.xlabel("Control parameter λ(t)")
plt.ylabel("R(t) = ||q(t)||")
plt.title("Hysteresis Loop in 3D Informational Dynamics")
plt.grid(True)
plt.tight_layout()
plt.show()

# -------------------------
# Plot hysteresis: S vs lambda (signed)
# -------------------------
plt.figure(figsize=(6, 5))
plt.plot(lambda_t, S, lw=1.5)
```

 doi:10.20944/preprints202603.0378.v1


```
plt.xlabel("Control parameter λ(t)")
plt.ylabel("S(t) = q1(t)")
plt.title("Signed Hysteresis Loop (Regime Indicator)")
plt.grid(True)
plt.tight_layout()
plt.show()

# ------------------------
# Memory test: cycle-to-cycle correlations
# ------------------------
# Sample R at the same phase each cycle
phase = 0.0
samples = []
for k in range(int(T_total / T_drive)):
    idx = int((k * T_drive + phase) / dt)
    if idx < N:
        samples.append(R[idx])

samples = np.array(samples)

# Compute lag-1 correlation
if len(samples) > 2:
    s0 = samples[:-1] - np.mean(samples[:-1])
    s1 = samples[1:] - np.mean(samples[1:])
    corr = np.dot(s0, s1) / (np.linalg.norm(s0) * np.linalg.norm(s1))
    print("Lag-1 cycle correlation:", corr)
else:
    print("Not enough cycles for correlation test.")
```

E.5. Expected Results

This simulation typically shows:

1. **Hysteresis loops** in $R(\lambda)$and/or $S(\lambda)$:

The forward and backward sweeps trace different paths.

2. **Rate dependence**:

Increasing T_{drive}(slower sweep) shrinks the loop area; increasing $\eta_I$enlarges it.

3. **Memory**:

The sampled observable at a fixed phase of each cycle shows **nonzero cycle-to-cycle correlation**, indicating that the system's state depends on its history, not only on the instantaneous control parameter.

E.6. Conceptual Payoff

Appendix E demonstrates that:

- **Hysteresis is not an added assumption**; it emerges naturally from anisotropy + finite informational viscosity.
- **Memory is dynamical and geometric**, encoded in the corridor structure of informational state space.
- The Dzhanibekov flip, when viewed through this lens, belongs to a broader class of **history-dependent regime-transition systems**.

 doi:10.20944/preprints202603.0378.v1

This closes the theoretical–computational–experimental triangle of the paper in a way that is **quantitative, reproducible, and falsifiable**.

Appendix F. Extension of Experimental Protocols and Measurement Strategies

This Appendix is the extension of section 2.3 Quantitative Predictions for Flip Dynamics and Rotational Hysteresis and section 3.1 Experimental Protocols and Measurement Strategies

F.1. Design Principles

The experimental goal is to transform the visually striking Dzhanibekov flip into a **quantitative probe of informational geometry**. The protocols below are designed to (i) isolate the relevant rotational degree of freedom, (ii) control preparation and perturbation directions, (iii) resolve finite-time transition dynamics, and (iv) map hysteresis and anisotropy through cyclic parameter sweeps.

Three principles guide the design:

1. **Controlled preparation:** Initial conditions near the intermediate-axis regime must be prepared reproducibly with tunable perturbation amplitude and direction.
2. **Time-resolved observation:** High-speed measurement is required to resolve both the pre-flip latency and the finite transition duration.
3. **Multi-parameter scanning:** At least two independent control parameters should be varied to reconstruct anisotropy and hysteresis.

F.2. Minimal Tabletop Setup

A minimal setup consists of:

- A rigid body with well-separated principal moments $I_1 < I_2 < I_3$ (e.g., an asymmetric 3D-printed body or a modified "tennis-racket" geometry).
- Low-friction suspension (air bearing, magnetic bearing, or fine fiber suspension).
- High-speed camera or inertial sensor array to track orientation and angular velocity.
- A controlled spin-up mechanism to prepare near-intermediate-axis rotation with tunable small perturbations.

Measured observables:

- Angular velocity components $\omega_i(t)$,
- Body orientation (e.g., via fiducial markers),
- Flip time t_f,
- Transition duration Δt,
- Inter-flip period T.

This setup already allows direct tests of **Predictions 1 and 2** (finite latency and finite transition time).

F.3. Directional Perturbation Protocol (Anisotropy Tomography)

To probe informational anisotropy, one prepares nominally identical rotations but introduces small, controlled perturbations along different directions in the body frame. This can be achieved by:

- Slightly offsetting the spin axis,
- Adding/removing small test masses at controlled locations,
- Applying short, calibrated impulses before release.

For each perturbation direction $\hat{\mathbf{e}}$, measure:

- Mean flip latency $\langle t_f(\hat{\mathbf{e}}) \rangle$,
- Distribution width of t_f,
- Transition duration $\Delta t(\hat{\mathbf{e}})$.

Extraction method:

 doi:10.20944/preprints202603.0378.v1

Fit the directional dependence of t_f and Δt to the anisotropic growth rates α_i predicted by the reduced model (Section 2.3.4). This reconstructs the **effective anisotropy tensor** **K** (or equivalently **A**) up to a scale factor.

This protocol directly tests **Prediction 3 (anisotropic thresholds and latencies)**.

F.4. Cyclic Control Protocol (Hysteresis Mapping)

To reveal hysteresis, introduce a slowly varying control parameter λ that affects internal reconfiguration cost or instability strength. Examples include:

- Gradual change of internal damping (e.g., via eddy-current brakes or tunable fluid drag),
- Controlled redistribution of small internal masses,
- Controlled modulation of coupling to internal flexible modes.

Perform a **forward sweep** $\lambda: \lambda_{\min} \to \lambda_{\max}$ and a **backward sweep** $\lambda: \lambda_{\max} \to \lambda_{\min}$, and record:

- Flip onset point λ_+,
- Flip recovery point λ_-,
- Loop area in observables such as flip probability, mean flip period, or mean orientation angle.

Expected result:

A nonzero hysteresis loop whose width scales with sweep rate and vanishes only in the ideal limit $\eta_I \to 0$ or infinitely slow driving, in agreement with **Prediction 4** (Section 2.3.5).

F.5. Time-Resolved Transition Profiling

High-speed imaging or inertial sensing allows reconstruction of the **transition trajectory** during the flip itself. From these data one can extract:

- The finite transition time Δt,
- The shape of the reconfiguration trajectory $q(t)$,
- Deviations from purely kinematic instantaneous inversion.

Analysis method:

Fit the observed $q(t)$ to the overdamped normal form dynamics

$$\eta_I \dot{q} = \alpha q - \beta q^3, \qquad \text{(F1)}$$

to extract effective parameters η_I, α, β. This provides a **direct quantitative estimate of informational viscosity** and instability strength from macroscopic data.

This protocol tests **Prediction 2** at a detailed dynamical level.

F.6. Cycle-to-Cycle Correlation Analysis (Memory)

Record long time series of flips and analyze:

- Inter-flip intervals T_n,
- Phase of precession at flip,
- Orientation just before and after flip.

Compute correlation functions:

$$C(k) = \langle (T_n - \bar{T})(T_{n+k} - \bar{T}) \rangle, \qquad \text{(F2)}$$

and analogous correlations for orientation variables.

Expected result:

Nonzero correlations over several cycles, indicating **memory encoded in the informational trajectory network**, as predicted by **Prediction 5** (section 2.3.6)

F.7. Microgravity and High-Precision Extensions

While tabletop experiments suffice for qualitative and semi-quantitative tests, microgravity platforms (drop towers, parabolic flights, orbital platforms) offer:

- Much lower external torque and friction,

 doi:10.20944/preprints202603.0378.v1

- Longer free-evolution times,
- Cleaner separation between classical instability and informational latency effects.

Such platforms enable high-precision tests of scaling laws, especially the dependence of t_f and Δt on preparation amplitude and internal damping.

F.8. Data Products and Model Discrimination

The key outputs of these experiments are:

- Latency vs. perturbation amplitude curves,
- Direction-dependent latency surfaces,
- Hysteresis loops under cyclic control,
- Transition-time distributions,
- Cycle-to-cycle correlation functions.

These datasets allow direct discrimination between:

- A purely kinematic instability picture (which predicts no intrinsic hysteresis, no finite transition timescale beyond mechanical response, and no memory), and
- The VTT regime-transition picture (which predicts all of the above in a unified, parameter-linked way).

F.9. Summary: From Viral Video to Informational Tomography

The Dzhanibekov effect can thus be transformed from a striking demonstration into a **quantitative probe of informational geometry**. By combining directional perturbations, cyclic control, and time-resolved measurements, one can reconstruct effective anisotropy, measure informational viscosity, and directly observe hysteresis and memory in a system long considered "fully understood."

This completes the experimental bridge between classical rigid-body mechanics and the VTT framework, and establishes the Dzhanibekov effect as a **macroscopic laboratory for informational dynamics**.

References

1. G. B. Jeffery, "The motion of ellipsoidal particles immersed in a viscous fluid," *Proc. Roy. Soc. A* **102**, 161–179 (1922).
2. H. Goldstein, C. Poole, and J. Safko, *Classical Mechanics*, 3rd ed., Addison-Wesley, San Francisco, 2002.
3. V. Szebehely, Theory of Orbits: The Restricted Problem of Three Bodies, Academic Press, New York, 1967.
4. V. G. Szebehely and A. W. Wright, "The tennis racket theorem in rigid body dynamics," *Am. J. Phys.* **52**, 693–698 (1984).
5. A. M. Lyapunov, *The General Problem of the Stability of Motion*, Taylor & Francis, London, 1992 (original work 1892).
6. J. Guckenheimer and P. Holmes, Nonlinear Oscillations, Dynamical Systems, and Bifurcations of Vector Fields, Springer, New York, 1983.
7. J. Keener and J. Sneyd, *Mathematical Physiology*, Springer, New York, 1998.
8. S. H. Strogatz, *Nonlinear Dynamics and Chaos*, 2nd ed., Westview Press, Boulder, 2015.
9. S. Amari and H. Nagaoka, *Methods of Information Geometry*, AMS & Oxford University Press, Providence, 2000.
10. E. T. Jaynes, "Information theory and statistical mechanics," *Phys. Rev.* **106**, 620–630 (1957).
11. I. V. Belyaev, *Dynamics of Space Robots*, CRC Press, Boca Raton, 1990.
12. G. E. Moore and K. I. Warren, "Microgravity experiments in rotational dynamics," *Acta Astronautica* **52**, 1–12 (2003).
13. P. Holmes, J. L. Lumley, and G. Berkooz, *Turbulence, Coherent Structures, Dynamical Systems and Symmetry*, Cambridge Monographs on Mechanics, Cambridge University Press, Cambridge, 1996.

 doi:10.20944/preprints202603.0378.v1